compared for HDR and LDR cases for structures used in planning for both approaches. Target V200, V150, V100, V95, D90, rectum V100, rectum D2cc, and rectum D1cc were compared between LDR and HDR patients. Due to HDR plans being nested within patients, significance (p) was determined using a linear mixed effects model with random intercepts for each patient. $P<0.05$ was considered statistically significant.

Results: The study cohort consisted of 112 patients treated from 2012-2016. 51 patients received LDR, 61 patients received HDR (100 total implants). 23 patients had brachytherapy as a boost. 91 (81.2%) had cT1a-c disease, and 21 (18.8%) had cT2a-c disease. Gleason score 6, 7, and 8-10 were present in 52 (46.4%), 52 (46.4%), and 8 (7.2%) patients. 41 (36.6%) and 57 (50.9) had low and intermediate risk disease, respectively. Median pre-treatment PSA was 6.43 (interquartile range [IQR] 4.93-9.29). As described in the table, patients receiving HDR had lower target V200, V150, V100, and V95, while there was no difference in D90. Rectum D2cc was similar between LDR and HDR, but rectum D1cc was lower in the HDR group. Rectum V100 was zero for all patients with HDR, and higher for LDR.

Conclusions: In our series of patients treated by the same brachytherapists, patients receiving HDR brachytherapy had lower V150 and V200 within the target, and lower rectal doses compared to our LDR patients. Target coverage was also better in the HDR patients, although D90's were similar.

Table

	HDR	LDR	p
Mean Target V200% (Standard Error [SE])	7.69 (0.62)	13.83 (0.74)	<.0001
Mean Target V150% (SE)	29.06 (1.29)	43.20 (1.54)	<.0001
Mean Target V100% (SE)	96.05 (1.79)	83.15 (2.04)	<.0001
Mean Target V95% (SE)	97.95 (0.33)	93.42 (0.42)	<.0001
Mean Target D90 [% of prescription] (SE)	106.82 (0.99)	105.64 (1.45)	.50
Mean Rectum D 2 cc Gy [% of prescription] (SE)	66.18 (1.19)	67.95 (1.52)	.36
Mean Rectum D 1 cc Gy [% of prescription] (SE)	71.64 (1.32)	81.71 (1.68)	<.0001
Mean Rectum V100% [cc] (SE)	0 (0)	0.46 (0.04)	-

PO127

Twice vs Single Applications in High Dose Rate Brachytherapy (HDR) Boost. Same Results in High Risk Prostate Cancer Patients?

Silvia Rodriguez Villalba, PhD, MD, Antonio Otal Palacin, PhD, Jose Richart Sancho, MPh, Jose Perez-Calatayud, MPh, Manuel Santos Ortega, PhD, MD, Carolina Domingo, PhD, MD. Radiation Oncology, Hospital Clinica Benidorm, Benidorm, Spain.

Purpose: HDR brachytherapy (BT) boost is utilized for dose escalation in the treatment of clinically localized high risk prostate cancer. We report two different regimens, 2 aplications of 9,5 Gy related to one aplication of 15 Gy as a boost to external beam radiotherapy (EBRT) in a large cohort of patients treated in a single institution.

Materials and Methods: We reviewed retrospectively data of 95 patients treated for clinically localized prostate cancer, High risk patients (D'Amico classifications) with curative intent between August 2009 and December 2015. All patients received either IMRT pelvic radiotherapy (Median 50,4 Gy) in combination with a HDR in two regimens: 2 fractions of 9,5 Gy (69 patients. 73%) separated one week before May of 2014 or a single fraction of 15 Gy (26 patients. 27%) after these date.Treatment was delivered using an out-patient intraoperative ultrasound-based technique with the patient under spinal anesthesia and sedation. BT boost was administrated 3-4 weeks after finishing EBRT according our protocol in all the patients.

Results: Median age 59 years (51-82 y). Median Gleason 7 (3-10) and median value of PSA at diagnosis 11 ng/ml (2, 26-106 ng/ ml). Fifty patients (16%) were diabetic, 49 (52%) high blood pressure and 16 (17%) were under an anticoagulant treatment. Eighty five patients (95%) were staged with a magnetic resonance (MRI). Ninety four patients (99%) received androgen deprivation (AD) and 29 (31%) as neoadjuvant treatment. Median AD was 24 months (5-24 m). All patients had a personally follow-up. Follow-up assessment was with CTCAE v.4 and blood test with PSA at 12 weeks, every 4 months for the first year and then every 6 months. After 5 years of follow up, it is done once a year. Median follow-up is 39 months (8-83 m). At December of 2016, 83 patients (87%) are alive without disease, 2 (2%) have died of tumor and 10 patients (11%) have died of other causes. Overall survival at 12, 24 and 60 months are 99, 96 and 96% % respectively for the patients treated with 2 fractions and 100 % at 12 and 24 months for patients treated with a single fraction without statistical significance (p NS). Biochemical control is 100% in both groups. Local control is 100% in both groups, lymph node control is 99% (one retroperitoneal recurrence in a patient treated with 2 fractions) and 4 patients have bone metastases (all patients treated with 2 fractions regimen) without statistical significance (p NS). There is not acute genitourinary (GU) or gastrointestinal (GI) toxicity grade 3. One patient (1%) needed a transurethral resection because chronic obstruction and another surgical treatment of urethral stenosis. Five patients (5%) developed rectitis grade 3 (3 treated with 2 fractions of 9,5 Gy and one patient treated with 1 fraction of 15 Gy) in a median time of 8 months (3-29 m). All of them were solved with Argon laser. There are not difference in adverse grade 3 rectal events between both groups (p = NS). Due to the low number of other toxicities reported in follow-up, multivariate analysis was not done.

Conclusions: Prostate HDR boost delivered in a single 15 Gy treatment fraction compares favorably in terms of toxicity to 2 fractions of 9.5 Gy, one week apart. Longer follow-up is needed to compare clinical results in terms of overall survival and local control.

PO128

Clinical Application of Pre-Treatment Image Verification of Catheter Positions for HDR Prostate Brachytherapy

Ryan L. Smith, MAppSc[1], Annette Haworth, PhD[2], Max Hanlon, BSc[3], Bronwyn Matheson, MD[1], Jeremy Millar, MD[1], Vanessa Panettieri, PhD[1], Rick Franich, PhD[3]. [1]Alfred Health Radiation Oncology, The Alfred Hospital, Melbourne, Australia; [2]School of Physics, University of Sydney, Sydney, Australia; [3]School of Science, RMIT University, Melbourne, Australia.

Purpose: Swelling of the prostate and perineum occurs and over the time period between imaging (*for treatment planning*) and treatment delivery, causing the catheter positions (and hence displaced planned source dwell positions) to potentially shift relative to the anatomy. Displaced catheter positions unaccounted for at treatment can produce a perturbed dose distribution relative to the prostate and surrounding organs at risk. Re-imaging the patient, ideally in the treatment bunker, prior to treatment delivery is desirable in order to verify the position of the catheters relative to the surrounding anatomy. We have established a pre-treatment imaging approach using our Brachytherapy Image Guided Verification (BIGV) system. Pre-treatment image verification of the catheter positions are performed in the treatment bunker and compared directly to the treatment planning system. In this work we present the clinical results for 14 HDR prostate patients, where pre-treatment verification was performed on images acquired immediately prior to treatment delivery.

Materials and Methods: Pre-treatment imaging was performed for 28 treatment fractions, (2 fractions per patient) with the positions of the implanted catheters at each treatment fraction verified using the BIGV system. This system which consists of a flat panel detector (FPD) embedded into the brachytherapy treatment couch and a ceiling suspended x-ray device. The patient was setup on the treatment couch and aligned above the sensitive region of the FPD. Radio-opaque x-ray markers were inserted into the plastic proguide catheters in order to verify the positions relative to previously implanted gold prostate fiducial markers. The ceiling suspended x-ray system was positioned above the patient and an anterior-posterior (A-P) x-ray image was acquired with the FPD. The gold prostate fiducial markers were identified and registered with the markers identified in the treatment plan. A comparison of planned and measured catheter positions was then performed relative to the prostate. Catheter tip positions were compared and the agreement of the catheter path through the prostate region was evaluated for all catheters with inserted x-ray markers. Observed catheter displacements at treatment were re-created on the treatment plan to assess any dosimetric impact.

Results: The average registration uncertainty between the A-P image and the TPS for the gold fiducial markers was 0.9 mm (s.d.0.4 mm, max 1.7 mm). The

largest catheter displacement was observed for fraction 1 with an average catheter tip displacement in the inferior direction of 10.8 mm. The average inferior catheter tip displacement for fraction 2 was 1.5 mm (s.d. 0.9 mm, max. 3.3 mm). The catheter paths through the prostate region agreed to within 2mm, as shown in figure 1 (blue planned, red measured catheter paths), suggesting minimal lateral displacement of the catheter positions.
Conclusions: Pre-treatment imaging has been performed to verify catheter positions, with the patient in the treatment position, immediately prior to treatment delivery. The measured catheter displacements observed for fraction 1 were on average greater than fraction 2, and suggests the rate of perineum swelling is important and may result in a deviated dose distribution. The BIGV system which enables direct comparison of planned catheter positions with measured positions, immediately prior to treatment, permit the introduction of adaptive planning techniques in HDR prostate brachytherapy.

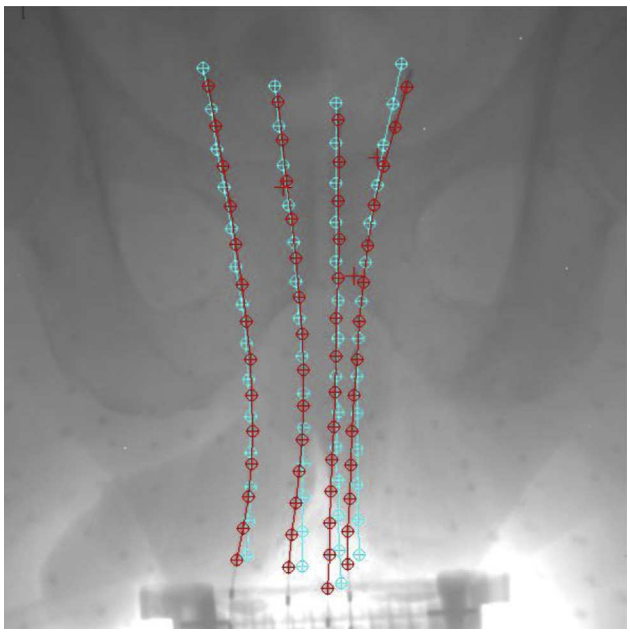

PO129

Focal Radiosensitization of Brachytherapy: Determining the Optimal Design of Drug Eluting Implants

Christian V. Guthier, Ph.D.[1], Anthony V. D'Amico, M.D., Ph.D.[1], Martin T. King, M.D., Ph.D.[1], Paul L. Nguyen, M.D.[1], Peter F. Orio, M.D.[1], Srinivas Sridhar, Ph.D.[1,2], G. Mike Makrigiorgos, Ph.D.[1], Robert A. Cormack, Ph.D.[1] [1]Department of Radiation Oncology, Brigham and Women's Hospital and Dana-Farber Cancer Institute, Boston, MA, USA; [2]Department of Physics, Nanomedicine Science and Technology Center, Northeastern University, Boston, MA, USA.

Purpose: In-situ drug release concurrent with radiation therapy has been proposed as a means to enhance the therapeutic ratio of permanent prostate brachytherapy. Both brachytherapy sources and brachytherapy spacers have been proposed as potential eluters to release drugs directly into the prostate. This work models the biologic effect of implantable eluters of radio-sensitizer in conjunction with brachytherapy to determine which of the proposed methods is the preferred delivery approach.
Materials and Methods: The combined effect of implanted drug eluters and radioactive sources were modeled in a manner that allowed selection of eluter location to optimize biologic effect for a range of model parameters. The retrospective study includes 20 patients previously treated with LDR brachytherapy from which prostate geometries, source and spacer positions were extracted. The biological effect of drug concentrations was calculated by using the steady state solution to the diffusion equation including an elimination term characterized by the diffusion-elimination modulus (φ_b). Radiosensitization was assumed to be dependent on drug concentration up to a saturation concentration (c_{sat}). For a given number of eluters (n_e) the clinical objective was to find the best possible configuration of eluters, for a given drug delivery vehicle that maximizes the biological effect.
Results: The biologic effect was calculated for prostate volumes from 11 cm^3 to 64cm^3, φ_b from 0.01 mm^{-1} to 1 mm^{-1}, c_{sat} from 0.05 to 8.0 times the steady state drug concentration released from the surface of the eluter and n_e from 10 to minimum number of either number of used spacers or seeds. For the parameter space of (φ_b,c_{sat})=([0.01, 0.25],[0.05, 4]) that results in a large fraction of the gland being maximally sensitized, drug eluting spacers or sources produce equal increase in biologic effect. For the remaining (φ_b,c_{sat})-space eluting spacers are preferable. Placing drug eluting implants in planned locations throughout the prostate results in even greater sensitization than using only source or spacer locations .
Conclusions: Drug eluting brachytherapy spacers offer a means to increase the biologic effect of brachytherapy implants with no change in treatment process. Incorporating additional needle placements to allow the freedom to place spacers independently of source placement offers a means to increase the therapeutic ratio with relatively minor modifications of the implant process.

PO130

Single Fraction High Dose Rate Brachytherapy as Monotherapy in Intermediate Risk Prostate Cancer: Early Clinical Outcomes

Raghavendra Gowda, FRANZCR, Jehan Titus, FRACS, Eric Yeoh, FRANZCR, John Lawson, M Sc CMPS, Evangelos Katsilis, B Med.Rad (RT). Royal Adelaide Hospital, Adelaide, Australia.

Purpose: To report early urinary (GU), gastrointestinal (GI) adverse events (AEs) and PSA outcomes after single fraction high dose rate brachytherapy as monotherapy (HDR-M) for intermediate risk (NCCN risk category) prostate cancer using real-time trans-rectal ultrasound (TRUS) based planning.
Materials and Methods: Between April 2015 and September 2016, a total of 40 consecutive patients with intermediate risk prostate cancer were treated with a single fraction of 19 Gy (n=10) or 20 Gy (n=30) HDR-M. None received hormone therapy Real time US based planning technique was used. Genito-urinary (GU) and gastro-intestinal (GI) toxicity were assessed using the International Prostate Symptom Score scale (IPSS) and RTOG scales (GI/GU) scales. Biochemical relapse was defined according to the Phoenix Consensus definition (PSA nadir + 2µg/L).
Results: Median age was 69y (range, 51y-84y) and median follow up was 9 months (range, 3-22 months). All patients tolerated the procedure well with no intraoperative or perioperative complications. No patient developed urinary retention. Five (12.5%) patients developed Grade 2 urinary toxicity which returned to baseline by 3 months. There was no $\geq$ Grade3 urinary toxicity (including urinary strictures). Median IPSS at baseline was 6 , increased to 9 at 1month , returning to 6 at 3months. No patient developed any Grade of GI toxicity. After a median follow up of 9 months there were no biochemical failures. Cumulative percentage of patients with PSA $\leq$ 1 ml at 6 months was 30% with PSAs continuing to fall in all patients as of last follow up. Median percentage PSA fall at 1, 3, and 6 months was 47%, 70% and 79% respectively compared to iPSA.
Conclusions: This is the first report of the use of single fraction HDR brachytherapy as monotherapy in prostate cancer from Australia. This treatment is well tolerated with early results showing low GU/ GI adverse events and good early PSA outcomes. Longer follow up is needed to assess long-term outcomes and toxicities.

Mobius3D

THE COMPLETE PATIENT QA SYSTEM

- **3D PATIENT PLAN QA**
- **3D IMRT/VMAT PRE TREATMENT QA**
- **3D *IN VIVO* DAILY TREATMENT QA**
- **ONLINE PATIENT POSITIONING QA**

Upgrade your patient safety by bridging the gap between patient QA and machine QA:

DoseLab, the complete TG-142 solution, is now integrated into Mobius3D!

Visit mobiusmed.com/mobius3d to learn more or register for a bi-weekly webinar at mobiusmed.com/webinars

MOBIUS MEDICAL SYSTEMS
INNOVATIVE SOFTWARE FOR MODERN RADIATION ONCOLOGY

On the use of C-arm fluoroscopy for treatment planning in high dose rate brachytherapy

Lizhong Liu,[a] Daniel A. Bassano, Satish C. Prasad, Bonnie L. Keshler, and Seung S. Hahn
Department of Radiation Oncology, SUNY Upstate Medical University, Syracuse, New York 13210

(Received 13 March 2003; revised 4 June 2003; accepted for publication 19 June 2003; published 15 August 2003)

Treatment planning for brachytherapy requires the acquisition of geometrical information of the implant applicator and the patient anatomy. This is typically done using a simulator or a computed tomography scanner. In this study, we present a different method by which orthogonal images from a C-arm fluoroscopic machine is used for high dose rate brachytherapy treatment planning. A typical C-arm is not isocentric, and it does not have the mechanical accuracy of a simulator. One solution is to place a reconstruction box with fiducial markers around the patient. However, with the limited clearance of the C-arm this method is very cumbersome to use, and is not suitable for all patients and implant sites. A different approach is adopted in our study. First, the C-arm movements are limited to three directions only between the two orthogonal images: the C-orbital rotation, the vertical column, and the horizontal arm directions. The amounts of the two linear movements and the geometric parameters of the C-arm orbit are used to calculate the location of the crossing point of the two beams and thus the magnification factors of the two images. Second, the fluoroscopic images from the C-arm workstation are transferred in DICOM format to the planning computer through a local area network. Distortions in the fluoroscopic images, with its major component the ''pincushion'' effect, are numerically removed using a software program developed in house, which employs a seven-parameter polynomial filter. The overall reconstruction accuracy using this method is found to be 2 mm. This filmless process reduces the overall time needed for treatment planning, and greatly improves the workflow for high dose rate brachytherapy procedures. Since its commissioning nearly three years ago, this system has been used extensively at our institution for endobronchial, intracavitary, and interstitial brachytherapy planning with satisfactory results. [DOI: 10.1118/1.1598851]

Key words: high dose rate brachytherapy, treatment planning, C-arm, fluoroscopy, image distortion.

INTRODUCTION

Afterloading brachytherapy performed using the low dose rate (LDR) technique typically involves the following steps: placement of the implant applicator or catheters in the operating room, imaging studies on a simulator or computed tomography (CT) scanner, treatment planning calculations, and radioactive source insertion and treatment in a controlled patient room. With high dose rate (HDR) remote afterloaders becoming widely available during the last decade, afterloading brachytherapy is now routinely performed using both the traditional LDR and the newer HDR technique. Apart from the differences in dosimetry, radiobiology, and radiation protection, HDR brachytherapy has the advantage that certain procedures, such as the endobronchial and intracavitary implants, can be performed in the same room thus eliminating the need for patient transport and the possibility of applicator displacement. This is achievable only for institutions with a dedicated HDR procedure room equipped with a fluoroscopy x-ray machine. The fluoroscopy machine is essential for guiding and verifying the placement of implant catheters or applicator, and its images must be suitable for treatment planning purpose. One fluoroscopy machine satisfying this requirement is commercially available through one HDR vendor (Nucletron Corporation, Columbia, Maryland) as part of an integrated brachytherapy unit (IBU). It has enough degrees of motion allowing for the positioning of the x-ray tube and image intensifier assembly in any orientation around the patient isocentrically, and its mechanical accuracy rivals that of a treatment simulator. However, the cost of such a machine is prohibitively high for most radiotherapy departments.

An alternative to the expensive IBU fluoroscopy machine is a mobile C-arm fluoroscopy machine. These machines are designed to meet the needs for various surgical, diagnostic, and interventional procedures, and they typically do not have the imaging and mechanical capabilities required for a treatment planning imaging device. Specifically, most mobile C-arms are not isocentric and their mechanical accuracy and stability is inferior to that of a treatment simulator. One exception to this is the recently introduced SIREMOBIL Iso-C mobile C-arm from Siemens Medical Solutions USA, Inc. (Malvern, Pennsylvania). This C-arm has true isocentric design with good mechanical stability, and it offers CT-like three-dimensional images as an option. Such a mobile C-arm, although more expensive than conventional ones, would be ideally suited for brachytherapy treatment plan-

ning. However, most mobile C-arms in clinical use today are the conventional nonisocentric type. In addition to the mechanical capabilities, fluoroscopy images from C-arms are distorted due to photocathode curvature and electron optics of the image intensifier,[1–3] and unlike some C-arms specifically designed for quantitative imaging such as digitally subtracted angiography the distortions in a mobile C-arm fluoroscopy system are typically not digitally corrected by the vendors. One solution to the nonisocentricity and mechanical accuracy issues facing a mobile C-arm is to place a reconstruction box with fiducial markers around the patient. We purchased such a reconstruction box from our HDR machine vendor (Varian Medical Systems, Inc., Palo Alto, California) and experimented with the box technique during the commissioning stage for our HDR treatment system. We soon realized that clearance was an issue with the C-arm and that the reconstruction box technique was not suitable for the localization of applicators for different patient sizes and implant sites. Another investigator[4] has reached the same conclusion with box from a different manufacturer. The classical solution of using a magnification ring placed on the patient skin while taking images is simply not accurate enough for brachytherapy treatment planning. It has been suggested[4] that a ruler with markers can be placed inside the patient near the implant site for obtaining magnification factors. This might work for well-selected cases such as a pelvic implant with ruler inserted in the rectum, but is in general not feasible for other implant sites.

In this study we present a new approach for utilizing the mobile C-arm fluoroscopy for treatment planning in brachytherapy. With our new reconstruction method, the nonisocentricity issue facing a mobile C-arm is solved by limiting its degrees of motion between two orthogonal images and by deriving the magnification factors from the geometric parameters and the allowed movements of the C-arm. The suboptimal mechanical accuracy and stability of the mobile C-arm is partially accounted for by these parameters and by the data entry process. Distortions in the fluoroscopy images are digitally corrected using a software program developed in house that employs a seven parameter polynomial filter. Since the commissioning nearly three years ago, this system has been in extensive clinical use in our institution for endobronchial, intracavitary, and some interstitial implants with satisfactory results.

The paper is organized in four sections. The materials and methods section describes the C-arm fluoroscopy machine, the reconstruction method, and the image distortion correction used in this study. Phantom test results and clinical applications are presented in the results and discussions section. And finally major conclusions of this study are summarized in the closing section.

MATERIALS AND METHODS

Mobile C-arm fluoroscopy machine and treatment planning system

The mobile C-arm x-ray machine used in this study is a model OEC 9800 surgical C-arm manufactured by GE OEC Medical Systems (Waukesha, Wisconsin). It has both fluoroscopy and spot x-ray capability. Its image intensifier (II) has a diameter of 12 inches featuring a $1k \times 1k$ digital resolution. The x-ray target to II distance is nominally 100 cm, and the clearance from the bottom of the target housing to the II is 80 cm. The workstation for the C-arm is Ethernet ready, allowing for the direct transfer of digital fluoroscopic images to a treatment planning computer through a local area network.

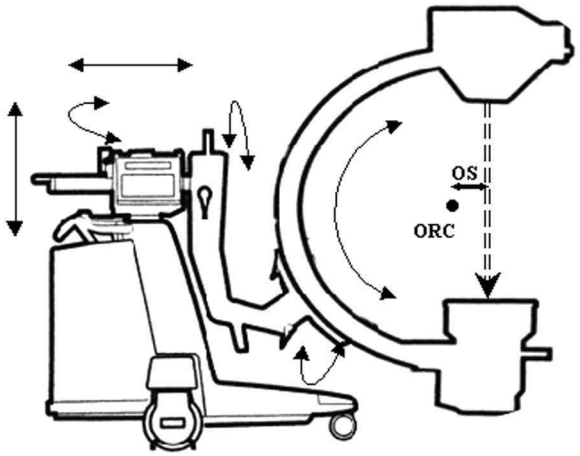

FIG. 1. Schematic drawing of the GE OEC 9800 mobile C-arm with its 6 degrees of motion. Sitting on top of the C-arm orbit is the x-ray target, and at the bottom is the image intensifier (II). The C-arm is not isocentric, with the central axis of the x-ray beam offset from the orbital rotation center (ORC) by an amount OS. Such a design provides adequate clearance in the lateral direction without increasing the C-arm orbit size.

The mobile C-arm is mechanically a very versatile machine. In addition to its roller wheels, there are 6 degrees of rotational and linear movements allowing for the proper positioning of the device around the patient. Figure 1 is a schematic drawing of the C-arm, illustrating its major components and movements. Shown on the top of the C-arm orbit is the x-ray target, and the II is at the bottom. Rotation in the plane of the C-arm orbit is allowed up to a maximum of 90 degrees counterclockwise and 25 degrees clockwise from the vertical anterior–posterior (AP) position shown in the figure. The C-arm orbit can also be flipped such that the target is on the bottom of the orbit, allowing for posterior–anterior (PA) orientation. Tilting of the C-arm orbital plane, and swiveling of the C-arm orbit and the horizontal cross arm are also possible. These rotational movements are complemented by two additional degrees of linear movements along the horizontal cross arm and the vertical column. Each of the two linear movements has a travel range of up to 20 cm.

The C-arm is not an isocentric machine in its orbital rotation plane, i.e., the central axis of its x-ray beam does not pass through a fixed point in space as the machine is being rotated along the C-arm orbit. As shown in Fig. 1, the C-arm orbital rotational center (ORC) is offset from the central axis beam by a distance, labeled OS in the figure. This offset is 10 cm for the C-arm in this study. The flip–flop rotation of the C-arm is, however, an isocentric motion, and its axis of rotation passes through the ORC (see Fig. 1).

The HDR brachytherapy treatment planning system used in this study is Varian BrachyVision 6.1 (Varian Medical Systems, Inc., Palo Alto, California), operating on a Windows NT platform. Digital images in DICOM as well as the generic JPEG, TIFF, and bitmap formats can be imported directly into BrachyVision. Following the transfer of the C-arm fluoroscopic images to the computer, distortions in these images are digitally corrected using a FORTRAN program developed in-house. The corrected DICOM images are imported into BrachyVision for treatment planning.

Although not adopted in our implementation, it is worthwhile to mention the reconstruction box method as provided by the HDR manufacturers. The reconstruction box method in general is mathematically precise, and is widely used in localizing intracranial targets[5] such as arteriovenous malformations. The fiducial markers on the box provide a reference frame, and the method is not dependent on the mechanical accuracy of the imaging device for reconstruction. In order to use the box method on other treatment sites such as the pelvis and lung, the reconstruction box has to be large enough, e.g., the box provided by our HDR manufacturer is 45 cm $\times$64 cm. With a clearance of 80 cm between the C-arm x-ray target housing and the II, such a large box placed on the patient table leaves no room to maneuver the C-arm without causing a collision. However, this is not to say that the reconstruction box method cannot be used on body sites other than the brain. With a portable or ceiling mounted x-ray machine, clearance is not an issue, and it is possible to position the machine freely around the box. Of course, such a machine would not have fluoroscopic capability.

Virtual isocenter reconstruction

Two x-ray images taken from different orientations are required for the three-dimensional reconstruction of the sources and structures in brachytherapy treatment planning. The orientations of the two images should be sufficiently apart, e.g., 40 degrees or greater, in order to have adequate reconstruction accuracy. There are clinical situations for which orthogonal images are necessary. For example, in the case of intracavitary cervical implant AP and lateral (LAT) images are needed in order to identify patient anatomical points such as the bladder and rectum.[6] Although the flip–flop rotation of the C-arm is an isocentric motion and utilizing image pairs taken with this rotation for reconstruction is straightforward, its rotational range is limited in the presence of the patient table, and this degree of motion is not suitable for imaging all implant sites. The nonisocentric C-arm orbital rotation is needed for an imaging technique that can meet all the clinical needs.

The difficulty with using a nonisocentric x-ray machine for imaging is ultimately the issue of determining the orientations and magnification factors of the two images. A new reconstruction method is developed and adopted in this study, which fully addresses these two issues for the mobile C-arm. This new method has two major components: (1) Among the 6 degrees of rotational and linear movements of the C-arm, only the orbital rotation and the two linear movements along the horizontal cross arm and vertical column are allowed between the two images; (2) The central axes of the two images cross at one point in space, and the location of this point can be determined using the geometric parameters of the C-arm orbit and the amounts of rotational and linear movements between the two images.

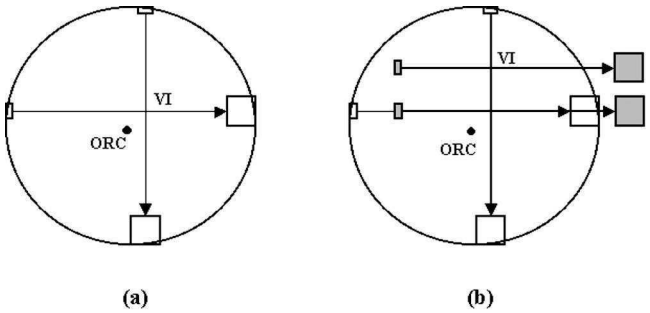

FIG. 2. The virtual isocenter reconstruction (VIR) method. (a) Rotating the C-arm in its orbital plane from the vertical AP to the horizontal LAT position. The two beams cross at a point away from the orbital rotational center. We term this crossing point the ''virtual isocenter'' (VI). (b) Allowing horizontal and vertical adjustments of the C-arm orbital plane between the two orthogonal images moves the VI to a new location. The horizontal adjustment changes the x-ray target to VI distance for the LAT beam, and the vertical adjustment changes that for the AP beam.

Figure 2 is an illustration of this method. The central axis of the x-ray beam is offset from the C-arm orbital rotation center (ORC) by an amount OS (see Fig. 1). As the x-ray target and II are rotated in the C-arm orbital plane from the vertical AP to the horizontal LAT position, the central axes of the AP and LAT beams cross at a point in space. This point is away from the ORC by an amount OS right lateral and OS superior, as shown in Fig. 2(a). We call this crossing point the ''virtual isocenter'' (VI). This displacement of the VI from the ORC results in a decrease for the target-VI distance for the vertical AP beam but an increase for the horizontal LAT beam. Allowing the C-arm two additional linear movements between the two images further changes the location of the VI. As shown in Fig. 2(b), the horizontal movement changes the target-VI distance for the LAT beam, and the vertical movement changes the target-VI distance for the AP beam.

Once the location of the VI is known, it is straightforward to determine the magnification factors of the AP and LAT images. They are simply the ratios of the target-II distance over the target-VI distance. With this information the three-dimensional reconstruction of the brachytherapy sources and structures is readily available with any modern treatment planning system. We term this method of using the C-arm images for treatment planning the ''virtual isocenter reconstruction'' (VIR) method.

Table I is a summary of the geometric parameters of the C-arm for the VIR method. Note that the target-II distance is dependent on the orientation of the C-arm, and this distance varies by as much as 2.3 cm between the PA and right lateral (RLAT) orientation. This is a direct result of the target and II sagging, and the mechanical imperfection of the C-arm. The target-VI distance is dependent on the linear movements in

TABLE I. Geometric parameters of the C-arm for the VIR method. See the text for details.

Orientation	Target-VI Distance (cm)	Target-II Distance (cm)
AP	59.5−UD	100.5
LLAT	79.5−LR	100.8
PA	78.9+UD	99.1
RLAT	59.8+LR	101.4

the horizontal (LR) and vertical (UD) directions between the LAT and AP or PA images, as discussed previously. Only two orthogonal image pairs, AP-LLAT and PA-RLAT, are allowed because of the limited orbital rotation range of the C-arm. It is not possible, for example, to have AP and RLAT as an image pair without using the flip–flop rotation of the C-arm (see Fig. 1), such a rotational movement is not allowed in the VIR method.

Several measurements are required in order to obtain the geometric parameters listed in Table I. The target-II distance is measured radiographically by placing a stainless steel ruler at a known distance from the II surface. From the magnification of the projected x-ray image at the II plane, the target-II distance can be calculated through $M = \mathrm{TID}/(\mathrm{TID}-\mathrm{D})$, where M is the magnification, TID is the target-II distance, and D is the ruler-II distance. The measurement of the target-VI distance is illustrated in Fig. 3. The center of II to the floor distance is measured for both the AP and LAT orientations, and the VI to II distance for the AP orientation is then the difference of the two. Similarly the VI to II distance for the LAT orientation is the difference of the center of II to the right wall distance between the AP and LAT orientations.

C-arm mechanical accuracy

The C-arm is not designed to be mechanically as accurate and stable as the treatment simulator. One indication of this is the orientation dependence of the target-II distance shown in Table I, a direct result of the target and II sagging. Another aspect of this is the relative shift of the target and the II in the plane perpendicular to the beam central axis, as shown in Fig. 4. Figure 4(a) is a fluoroscopic image taken with the C-arm in the AP orientation, and Fig. 4(b) in the LAT orientation. The larger dot in each figure is the projection of a BB placed on the target housing as a central axis indicator, and the smaller one is a BB placed at the center of the II plane. The relative positions of the two BBs appear shifted between the AP and LAT images. Such a shift is indication of the transverse movement of the II relative to the target. Figure 4(c) is a schematic drawing of the sagging induced relative movements of the target and II. In addition to the two linear movements discussed above, i.e., movements in the target-II direction and the transverse direction, it is also possible that sagging introduces a tilting of the II plane, as shown in Fig. 4(c).

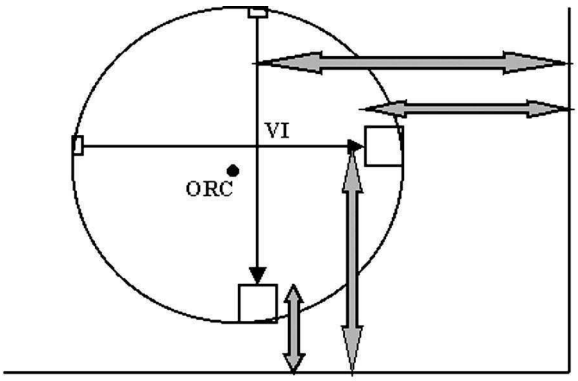

FIG. 3. Determination of the x-ray target to VI distance. The VI to II distance for the AP beam is the difference between the II to the floor distance for the LAT beam and that for the AP beam. Similarly, the VI to II distance for the LAT beam is the difference between the II to the right wall distance for the AP beam and that for the LAT beam.

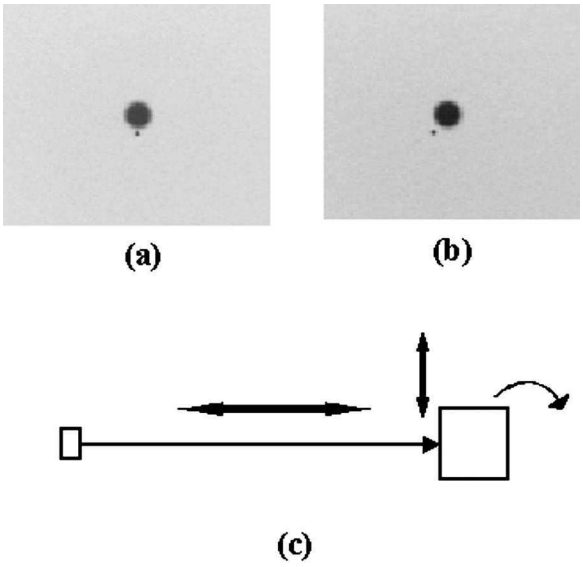

FIG. 4. Sagging induced relative movements of the x-ray target and II system. (a) Fluoroscopic image taken with C-arm in the AP orientation. The large dot is a BB placed on the x-ray target housing as a central axis indicator, and the small one is a BB placed at the center of the image intensifier plane. (b) Same as (a) but taken with C-arm in the LAT orientation. Note that the relative positions of the two BBs are shifted from that of (a). (c) Schematic drawing showing the relative movements of the x-ray target and II in the longitudinal and transverse directions. Also showing is a possible tilting of the II plane.

In the VIR method these mechanical imperfections of the C-arm are partially accounted for by using the orientation dependent target-II distance, shown in Table I, and by allowing small adjustment of the x-ray central axis indicator during data entry in the treatment planning system. Sagging induced tilting of the II plane is not accounted for in the current algorithm.

Image distortion correction

It is well known[1–3] that fluoroscopic images from the image intensifier are distorted. Figure 5(a) is an example of this distortion for a square Lucite plate placed on the II plane directly. The major component of the distortion is the ''pincushion'' effect, appearing as the stretch of corners for the

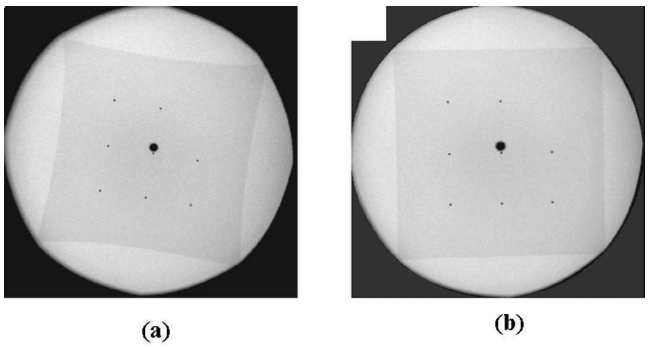

FIG. 5. (a) Uncorrected fluoroscopic image of a square plate placed on the image intensifier. (b) Distortion corrected image obtained using a seven parameter polynomial filter.

square object. The origin for this distortion is the curved shape of the photocathode and the electron optics inside the image intensifier. In addition, there is a rotational component to the distortion that is dependent on the orientation of the C-arm. This component has its origin in the earth magnetic field and stray magnetic field in the surroundings.

The distortion corrected image shown in Fig. 5(b) is obtained using a software program developed in house. This program employs a seven parameter polynomial filter shown below,

$$r = r'\left[1+\alpha\cdot\left(\frac{r'}{R}\right)^2+\beta\cdot\left(\frac{r'}{R}\right)^4\right],$$

$$\theta = \theta' + \delta_0 + \delta_1\left(\frac{r'}{R}\right) + \delta_2\left(\frac{r'}{R}\right)^2 + \gamma_x\cdot\frac{x'}{R}\cdot\left(1-\frac{|y'|}{R}\right) + \gamma_y\cdot\frac{y'}{R}\cdot\left(1-\frac{|x'|}{R}\right),$$

where R is the radius of the II, and α, β, δ_0, δ_1, δ_2, γ_x, and γ_y are the seven fitting parameters. (r',θ') and (x',y') are the polar and Cartesian coordinates of the raw image pixel, and (r,θ) is the polar coordinate of the distortion corrected image pixel. The pincushion effect is a distortion in the radial direction, and is described by the first polynomial. The two terms in the equation with parameters α and β are found to be sufficiently accurate for the C-arm in this study. For the distortion in the azimuth direction, the major component is the constant term, δ_0. The other higher order corrections represent spiral-like and parabolic-like distortions in the imaging plane.

The seven fitting parameters of the distortion correction program are obtained by analyzing the fluoroscopic images of a standard diagnostic imaging quality assurance test plate.

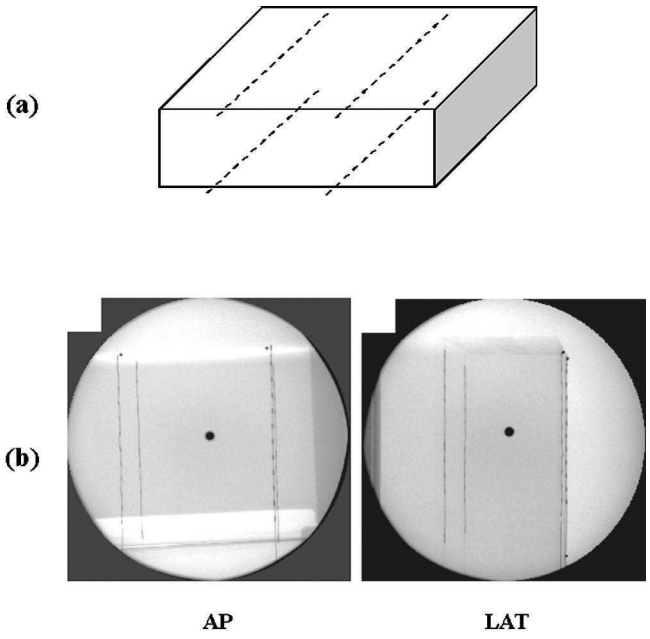

FIG. 6. (a) Test phantom constructed using four catheters taped to the top and bottom surfaces of a Styrofoam block. The catheters form a box of 10 cm wide, by 7 cm high, by approximately 13 cm long. (b) Distortion corrected AP and LAT images of the test phantom.

The rectangular Lucite plate with metallic square lattice pattern embedded is placed on the II plane, and fluoroscopic images are taken with the C-arm at different orientations. These images are analyzed using the correction program, and the fitting parameters are adjusted until the corrected images are satisfactory. Table II shows the values of these parameters for the different C-arm orientations. With these parameters, the average residual distortion error in the corrected image is 0.3 mm, and the maximum over the entire II plane is 1.0 mm. Such a degree of accuracy is acceptable for most brachytherapy treatment planning.

RESULTS AND DISCUSSION

Phantom test

In order to evaluate the overall accuracy of the reconstruction method, a test phantom is constructed using four plastic catheters. Two catheters are taped to the top of a Styrofoam block, and two to the bottom of the block. The four catheters form a box of 10 cm wide, by 7 cm high, by approximately 13 cm long. Figure 6(a) is a schematic drawing of this phantom. The plastic catheters are loaded with

TABLE II. Parameters used for image distortion correction. See the text for details.

Orientation	α	β	δ_0 (°)	δ_1 (°)	δ_2 (°)	γ_x (°)	γ_y (°)
AP	−0.1	0.003	8.0	−1.8	−0.9	−0.5	−0.3
LLAT	−0.1	0.003	6.5	−1.2	−1.2	1.0	−0.2
PA	−0.1	0.003	−1.5	1.8	0.9	0.7	0.0
RLAT	−0.1	0.003	0.0	1.2	1.2	−0.9	0.0

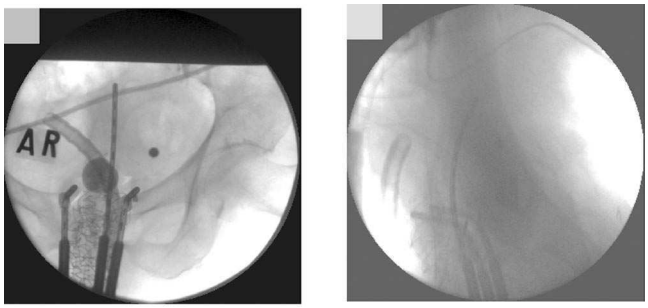

FIG. 7. Example of a Fletcher–Suite implant using the VIR method.

dummy ribbon seeds, and AP and LAT fluoroscopic images taken. These images are transferred to the BrachyVision treatment planning computer, and distortions in the images are digitally removed using the correction program. The corrected images, shown in Fig. 6(b), are then imported into the BrachyVision planning program, and the locations of the dummy seeds are reconstructed. The maximum reconstruction error over the entire phantom dimensions is found to be 2 mm. Such an overall degree of accuracy, which is the combined total of the residual image distortion in the II plane as discussed previously, the reconstruction algorithm, and the data entry process, is adequate for most HDR brachytherapy.

Clinical cases

The virtual isocenter reconstruction method using C-arm images has been in clinical use at our institution for nearly three years. Figure 7 is an example of its application in intracavitary Fletcher–Suite brachytherapy treatment planning. Table III is a summary of all the HDR brachytherapy implants performed at our institution during this time period. All treatment planning calculations, except for the case of vaginal cylinder implants, are done using either the C-arm VIR method or the conventional simulator and CT method. For vaginal cylinder implants the geometry is simple enough that no image is used for planning and C-arm fluoroscopy is used for verifying applicator placement in the AP direction only. For breast MammoSite (Proxima Therapeutics, Inc., Alpharetta, Georgia) treatment, CT is used for treatment planning and for verification of the placement, shape, and integrity of the applicator, and C-arm fluoroscopy is used for constancy checks of the applicator before each treatment fraction.

TABLE III. Summary of HDR implants performed from June 2000 to March 2003.

Implant type	No. of implants	Imaging device for planning
Endobronchial	45	C-arm
Esophageal	2	C-arm
GYN–Fletcher–Suite	6	C-arm
GYN–cylinder	79	(C-arm)
GYN–interstitial	1	CT
Sarcoma	12	Simulator
Head and Neck	6	C-arm, Simulator, CT
Breast–MammoSite	1	CT, (C-arm)
Total	152	

There are situations in which the simulator or CT scanner is the preferred imaging device, as indicated in Table III. These typically are large planar or volume implants for which the simulator offers the flexibility of arbitrary imaging orientation, and the CT simplifies catheter identification. In principle, the VIR method could also be extended to nonorthogonal imaging geometry. However, with the limited orbital rotational range of the C-arm and the metallic side bar of the patient table such an extension has little practical use.

The commissioning of the VIR method requires a significant effort by a physicist. For a partial commissioning, it is possible to use spot x-ray films instead of fluoroscopic images on the C-arm machine. Once commissioned, regular quality assurance checks on a quarterly or semiannual basis are required to maintain the overall performance of the system.

CONCLUSIONS

The virtual isocenter reconstruction method presented in this study offers a new practical solution for brachytherapy treatment planning using C-arm images. This method provides adequate geometric reconstruction accuracy, and eliminates the need for patient transport between applicator insertion and treatment delivery for HDR procedures such as endobronchial and intracavitary implants. The filmless process greatly reduces the overall time needed for treatment planning, and makes the overall HDR brachytherapy procedure a smooth process. This reconstruction method, however, does not replace conventional simulator and CT treatment planning, especially for large planar or volume implants and for implants that require nonorthogonal imaging geometry.

[a]Author to whom correspondence should be addressed; electronic mail: liul@upstate.edu

[1] S. Rudin, D. R. Bednarek, and R. Wong, "Accurate characterization of image intensifier distortion," Med. Phys. **18**, 1145–1151 (1991).
[2] E. Gronenschild, "Correction for geometric image distortion in the x-ray imaging chain: Local technique verses global technique," Med. Phys. **26**, 2602–2616 (1999).
[3] R. R. Liu, S. Rudin, and D. R. Bednarek, "Super-global distortion correction for a rotational C-arm x-ray image intensifier," Med. Phys. **26**, 1802–1810 (1999).
[4] A. Y. C. Fung, "C-arm imaging for brachytherapy source reconstruction: Geometrical accuracy," Med. Phys. **29**, 724–726 (2002).
[5] R. L. Siddon and N. H. Barth, "Stereotaxic localization of intracranial targets," Int. J. Radiat. Oncol., Biol., Phys. **13**, 1241–1246 (1987).
[6] ICRU, "Dose and volume specification for reporting intracavitary therapy in gynecology," ICRU Report No. 38, Bethesda, MD: International Commission on Radiation Units and Measurements, 1985.

Mobius3D

THE COMPLETE PATIENT QA SYSTEM

- **3D PATIENT PLAN QA**
- **3D IMRT/VMAT PRE TREATMENT QA**
- **3D *IN VIVO* DAILY TREATMENT QA**
- **ONLINE PATIENT POSITIONING QA**

Upgrade your patient safety by bridging the gap between patient QA and machine QA:

DoseLab, the complete TG-142 solution, is now integrated into Mobius3D!

Visit mobiusmed.com/mobius3d to learn more or register for a bi-weekly webinar at mobiusmed.com/webinars

MOBIUS MEDICAL SYSTEMS
INNOVATIVE SOFTWARE FOR MODERN RADIATION ONCOLOGY

C-Arm imaging for brachytherapy source reconstruction: Geometrical accuracy

Albert Y. C. Fung[a)]
Department of Medical Physics, Memorial Sloan-Kettering Cancer Center, New York, New York 10021

(Received 31 December 2001; accepted for publication 25 February 2002; published 11 April 2002)

We study the accuracy of brachytherapy source reconstruction using C-Arm images. We use a phantom embedded with dummy ribbons in a regular pattern, placed at the rotation center of the C-Arm. With a commercial reconstruction jig, radiographic films are taken without the image intensifier. The average error in reconstructed seed coordinates is 0.1 cm. However, the jig is inconvenient for patient procedures. For C-Arm reconstruction without the jig, the magnifications of the image intensifier along orthogonal directions are different. We ''stretch'' the image to equalize the magnifications. Afterward, seed reconstruction has an average error of 0.1 cm in all directions. © *2002 American Association of Physicists in Medicine.* [DOI: 10.1118/1.1473136]

Key words: geometrical, accuracy, C-Arm, brachytherapy, reconstruction

C-Arm mobile fluoroscopic units are generally considered inferior in geometrical accuracy of images for the purpose of radiation therapy planning, as evidenced by various articles recommending high-order polynomial correction for distortion.[1,2] However, there are clinical occasions in which the most convenient localization method is with a C-Arm. The original motivation of our project was to investigate the suitability of C-Arm reconstruction for treatment planning of high dose rate (HDR) brachytherapy of gynecological cancer, but it will be clear in later discussion that the result applies to other treatment sites. We studied the quantitative accuracy of seed reconstruction using C-Arm images, with and without a commercial reconstruction jig, and describe the result.

The C-Arm checked in our study is the General Electric OEC Series 9600 model. We used an in-house solid phantom to check the accuracy of C-Arm reconstruction. The phantom (Fig. 1) is made of acrylic slabs embedded with ribbons of metal seed dummies in a regular pattern. Five ribbons are arranged along the diagonal to avoid overlapping of individual ribbon images on orthogonal views. Each ribbon consists of dummies separated 1 cm apart. The phantom was placed at the rotation center of the C-Arm. Images were taken at anterior–posterior (AP) and left lateral directions. The same set of images were taken with and without a commercial jig (Fig. 2). (The jig was manufactured by Gammamed, MDS Nordion Haan GmbH, Bergische Str. 16, D-42781 Haan, Germany.) The jig consists of four transparent acrylic plates rigidly attached that surround the patient. On each plate are embedded radio-opaque markers at known positions. The jig also provides places to insert orthogonal film cassettes. The markers appear as circular dots on radiographic films. The marker positions were digitized together with the seeds, and ABACUS Version 3.1, the GammaMed software for HDR planning, was used in seed reconstruction. ABACUS calculates the seed positions based on the known (relative) coordinates of the markers. We have also reconstructed the seeds without using the jig and its markers, and just assuming orthogonal isocentric films.

We first discuss the general difficulties in reconstruction using images straightforwardly without a jig. (a) The Image Intensifier (II) of the C-Arm is not designed for perfect images. The image plane of the II is not well defined, and geometric distortion is well known. (b) Sagging due to the heavy II produces uncertainties in distances and angles between the x-ray source, the phantom, and the II. (c) The C-Arm rotation is not isocentric, even by design. As shown in Fig. 3, the source–axis distance is angular dependent. (d) The ABACUS software assumes we have actual-size images taken at the ''film'' location. The II images, whether digital ones on a computer screen or hard copies from the fluoroscope printer, have different magnifications from those at the II plane.

The jig resolves all of the above-mentioned problems. Radiographic films are taken without the II, thus bypassing its accompanying issues: distortion, ill-defined plane, and sagging. The film records actual-size images at fixed distances. The markers are the solution for nonisocentricity. Coordinates of the x-ray sources can be deduced from the digitized locations of the markers. The accuracy of seed reconstruction with the jig is excellent. Position of every reconstructed dummy seed is compared with the supposed position, and the average error in reconstructed seed coordinates is within 0.1 cm, which is acceptable for brachytherapy planning. However, the jig is 34×49 cm in dimension, rather small for many patients to fit in and in the way of the physician performing the procedure. It is also fragile, and can be easily bent or damaged during use. C-Arm has bulky II, which is difficult to maneuver under the patient couch. If posterior–anterior (PA) images were adequate, we could have the x-ray source below and the II above a supine patient. However, this jig requires an AP film, hence we would have to try pushing the II under the couch.

Hence, we also examined C-Arm reconstruction without the jig. The distances between various C-Arm components

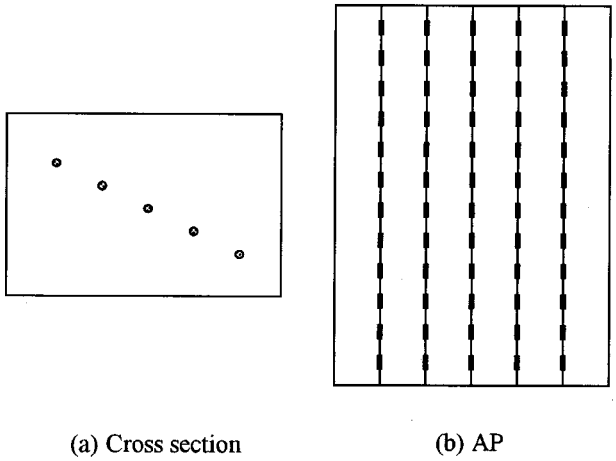

FIG. 1. In-house rectangular phantom with regularly spaced dummy seeds embedded. The phantom measures 30×12×6 cm. The figure is "figurative" in the sense that the number of seeds shown is different from the actual number on the phantom.

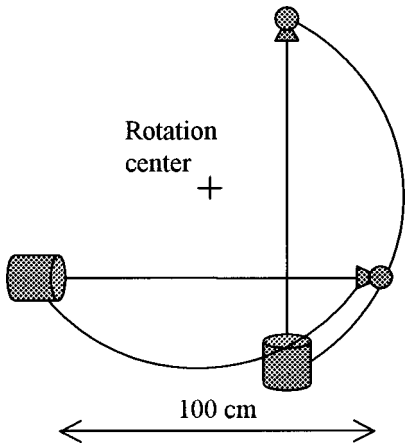

FIG. 3. Nonisocentric rotational geometry of C-Arm. The x-ray source and the II rotate on a common circular rail. The two locations drawn are for AP and lateral imaging. The "rotation center" is the center of the circular path. There is actually no "isocenter" of radiation.

were obtained from the manufacturer. The II images should be rescaled to the actual size at the II plane. In practice, we rescaled the images by one of the ribbons in the images. The scale was chosen so that the reconstructed seeds on the chosen ribbon have the correct separation, 1 cm. This canceled out first-degree error in distances and image magnifications. The ribbon was along the superior–inferior (SI) direction, perpendicular to the C-Arm rotation plane. The reconstructed seed coordinates had a mean error of 0.065 cm (standard deviation 0.025 cm) in the SI direction, but 0.2–0.3 cm along the other two orthogonal directions. We noticed that the diameters of the "circular" II and its images were in different proportions along various directions. Specifically, the II receptor had a diameter of 24.4 cm along the C-Arm rotation plane and 24.8 cm perpendicular. The circular rim on the images (the hard copies from the fluoroscope printer) measured 11.45 cm along the C-Arm rotation plane, and 10.8 cm perpendicular. This may be observed from Fig. 4, a to-scale image. Therefore, image magnifications along orthogonal directions were different by 7.7%. With a commercial graphic software that has image processing functions (such as Microsoft Paint), we modified the II images by "stretching" the image 7.7% perpendicular to the C-Arm plane. After changing the magnification in one direction, seed reconstruction became excellent in all directions, with a mean error of 0.59 cm (standard deviation 0.030 cm). Hence the main distortion of II images was this different magnification along orthogonal directions.

C-Arm distortion is known to be a function of the strength and direction of the Earth's magnetic field. The heavy II also causes sagging which is dependent on the orientation. In the study we used AP, PA, and lateral films. (Right and left laterals were taken with the same II position. The II could not rotate 180° along the rail, so we turned the whole C-Arm together with its base.) These represent the four extreme positions and orientations for the II. Hence, the result implies that reconstruction uncertainty is insignificant for any II orientation.

This reconstruction method assumes there is a ribbon perpendicular to the C-Arm rotation plane. For HDR brachy-

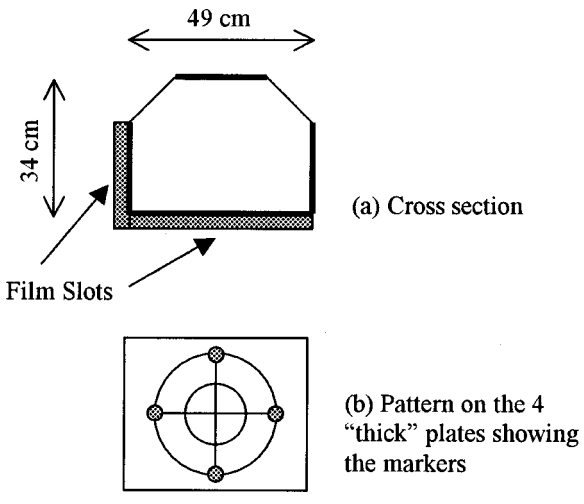

FIG. 2. Acrylic commercial reconstruction jig from Gammamed, with embedded radio-opaque markers on four "thick" plates.

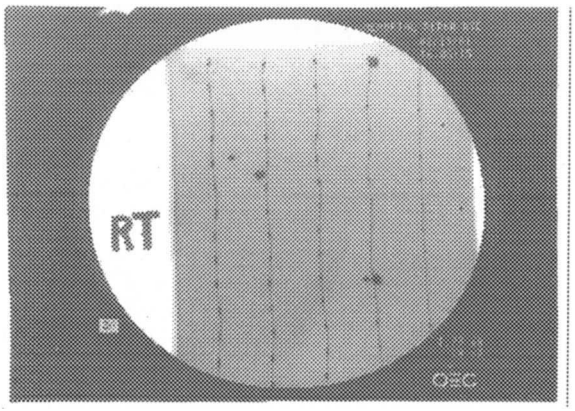

FIG. 4. AP image of the rectangular phantom taken with C-Arm fluoroscopy.

therapy of gynecological cancer one may use the dummy ribbon inserted into the patient's rectum. Our method will be useful for implants in other anatomical sites if (a) the patient is positioned such that dummy ribbons lie perpendicular to the C-Arm rotation plane, or (b) a scale (ring or ruler) is put on the patient with the known dimension perpendicular to the C-Arm rotation plane. One may estimate the error when the scale is not exactly perpendicular. Suppose the ribbon is 10° to the C-Arm rotation axis, the fractional error in length will be

$$\frac{1}{\cos 0^\circ} - \frac{1}{\cos 10^\circ} = 0.015. \quad (1)$$

An implant of maximum size 10 cm, if centered on the II aperture, will have the extreme points 5 cm from the center, and positional error at the extreme will be 0.75 mm, which is clinically acceptable.

In conclusion, we have studied the use of a C-Arm and a commercial jig in brachytherapy localization. The jig reduces reconstruction errors, but poses risk of being too small and easily damaged, and inconvenient for clinical use. The II images without a jig, however, may provide accurate reconstruction, if the images are stretched along one direction to give the same magnification as the other orthogonal direction.

[a)]Electronic mail: albert.fung@ahsys.org

[1] N. S. Cosby and K. W. Leszczynski, "Computer-aided radiation therapy simulation: Image intensifier spatial distortion correction for large field of view digital fluoroscopy," Phys. Med. Biol. **43**, 2265–2278 (1998).

[2] R. R. Liu, S. Rudin, and D. R. Bednarek, "Super-global distortion correction for a rotational C-arm x-ray image intensifier," Med. Phys. **26**, 1802–1810 (1999).

Original paper

Non isocentric film-based intracavitary brachytherapy planning in cervical cancer: a retrospective dosimetric analysis with CT planning

Kirti Tyagi, PhD[1], Hari Mukundan, MD[1], Deboleena Mukherjee, MSc[1], Manoj Semwal, PhD[2], Arti Sarin, MD[2]

[1]Radiation Oncology Centre, INHS Asvini, Colaba, Mumbai, India, [2]Radiotherapy Department, R&R Hospital, Delhi, India

Abstract

Purpose: To compare intracavitary brachytherapy dose estimation for organs at risk (bladder and rectum) based on semi-orthogonal reconstruction of radiographs on non-isocentric X-ray unit and Computed Tomography (CT) – based volumetric planning in cervical cancer.

Material and methods: Bladder and rectal points as per International Commission on Radiation Units and Measurements (ICRU) report 38, were retrospectively evaluated on 15 high dose rate intracavitary brachytherapy applications for cervical cancer cases. With the same source configuration as obtained during planning on radiographs performed on a non-isocentric X-ray unit, the mean doses to 2cc of most irradiated part of bladder and rectum were computed by CT planning and these estimates were compared with the doses at ICRU bladder and rectal points.

Results: The mean ICRU point dose for bladder was 3.08 Gy (1.9-5.9 Gy) and mean dose to 2 cc (D2cc) bladder was 6.91 Gy (2.9-12.2 Gy). ICRU rectal dose was 3.8 Gy (2.4-4.45 Gy) and was comparable with D2cc rectum dose 4.2 Gy (2.8-5.9 Gy). Comparison of mean total dose (ICRU point vs. D2cc) for each patient was found to be significantly different for bladder ($p = 0.000$), but not for rectum ($p = 0.08$).

Conclusions: On comparison of ICRU point based planning with volumetric planning on CT, it was found that bladder doses were underestimated by the film based method. However, the rectal doses were found to be similar to the D2cc doses. The results with non isocentric film based treatment planning were similar to the existing literature on orthogonal film based simulator planning.

J Contemp Brachyther 2012; 4, 3: 129-134
DOI: 10.5114/jcb.2012.30678

Key words: bladder dose, brachytherapy, cervical cancer, radiograph, rectal dose.

Purpose

High Dose Rate (HDR) brachytherapy in the treatment of cervical cancer with or without external radiotherapy is an essential component of management. It has a high therapeutic index delivering a high dose to primary cervical lesion and lower doses to adjacent organs [1-3]. In brachytherapy, an exact knowledge of the applicator geometry is necessary for an accurate calculation of dose to tumor and critical organs [4]. The traditional ways to reconstruct the brachytherapy catheters are either using a semi-orthogonal film method with a reconstruction jig or a pair of isocentric orthogonal or variable angle X-ray imaging method. X-ray images are obtained by using a therapy simulator or an integrated brachytherapy unit (IBU). Except IBU, the procedure requires that the patient is transferred after the application to the X-ray unit room for obtaining the reconstruction images and needs to be transported back to the brachytherapy treatment room to administer the irradiation. A modern approach in treatment planning for cervical cancer is based on Computed Tomography (CT) or Magnetic Resonance (MR) images and on a 3D dose calculation. Since 2004, several guidelines for image based brachytherapy for cervical cancer have been published [2,5,6].

At our centre, intracavitary brachytherapy (ICBT) planning has been carried with the 2D X-ray film method using a reconstruction jig and semi orthogonal reconstruction. The present study was carried out with the intention of changing over to CT based 3D planning. The treatments delivered using 2D film planning were also planned with CT imaging keeping the same source configuration. The doses to organs at risks i.e. bladder and rectum were computed by both the methods for further analysis. To our knowledge, there has been limited published data or literature available regarding the dosimetric comparison of semi orthogonal reconstruction of non isocentric X-rays with orthogonal X-rays or CT-MRI brachytherapy treatment planning in cervical cancers.

Address for correspondence: Kirti Tyagi, PhD, Medical Physicist, Radiation Oncology Centre, INHS Asvini, Colaba, Mumbai-400005, India, ✉ e-mail: callkirti@yahoo.com

Received: 23.04.2012
Accepted: 19.07.2012
Published: 27.09.2012

Material and methods

Patients selection

Ten patients with cervical cancer (Stage IIB – 4 patients, Stage IIIB – 4 patients, Stage IVA – 2 patients) who underwent 30 intracavitary brachytherapy insertions at our centre were included in this study. Treatment planning was done with conventional planning with a reconstruction jig. A preliminary study of CT guided volumetric planning has been performed retrospectively. This study was approved by the hospital's ethical committee.

Treatment scheme

The standard treatment protocol for cervical cancers at our centre consists of external beam radiotherapy (50 Gy/25 fractions) with concomitant chemotherapy and ICBT. After 7-10 days of completion of external chemo-radiotherapy to the pelvis, patients were taken for HDR-ICBT and a total dose of 21 Gy in three equal fractions of 7 Gy each at weekly intervals was given.

Brachytherapy insertion

The Fletcher Williamson applicators (Nucletron, Veenendaal, The Netherlands®) were used for intracavitary brachytherapy application consisting of uterine tandem and a pair of ovoids. Standard metallic applicators were used without special modification for CT/MRI compatibility. Before each application, a urinary catheter was inserted and the catheter balloon inflated with contrast and normal saline (7 ml) for visualizing the bladder. Appropriate packing was done to fix the applicator in position and to push the bladder and rectum away from the vaginal applicators. Bladder and rectal reference points were identified according to ICRU 38 recommendations. The patients were under conscious sedation.

Brachytherapy planning and treatment: conventional planning

After insertion of the applicators, X-ray images were taken with patient in supine position (AP and lateral views) for conventional planning with a reconstruction jig. To minimize patient movement during radiographs, the reconstruction jig base plate was kept below the patient and it remained there till the treatment was completed. The reconstruction jig (Fig. 1) was supplied by Nucletron® and comprises of a base plate and a C shaped mountable structure. The base and side plates are embedded with radio opaque markers at known positions. These markers appear as a straight line with circular dots on radiographic films. The X-ray tube is focused on the markers on upper C-shaped plate. The base plate also has a provision for holding the radiographic film cassettes for lateral as well as AP radiographs. The brachytherapy treatment planning systems require setup parameters, with magnification factors of the images. Semi orthogonal reconstruction method is used for reconstruction of the images. This method allows the use of a non isocentric X-ray unit to take the two reconstruction radiographs. Truly orthogonal orientations are not easily obtained with non isocentric X-ray unit. A localization jig with AP and lateral cross wires is placed over the patient and radiographs are taken. The semi orthogonal reconstruction method accepts X-rays beams whose central axes do not intersect and are not perpendicular to one another. The only requirement is that the projections of the cross-wires on the two corresponding box faces are visible on the radiographs (Fig. 2).

Geometrical reconstruction of applicator and dose computation was carried out using PLATO SUNRISE (Brachytherapy v14.3.5, Nucletron, The Netherlands®) brachytherapy treatment planning system using Vidar Dosimetry Pro scanner. The films were scanned with scanner. Point A was defined on the radiographs as being 2 cm superior (along the tandem) to the flange abutting external cervical os and 2 cm lateral from the axis of the tandem. The source positions were loaded as per the standard loading pattern in accordance with the Manchester System. These dwell positions were then optimized to minimize the dose to rectal and bladder points. The 7 Gy dose was prescribed to point A. The doses to point A, bladder and rectum were calculated. In the planning process, bladder and rectum point

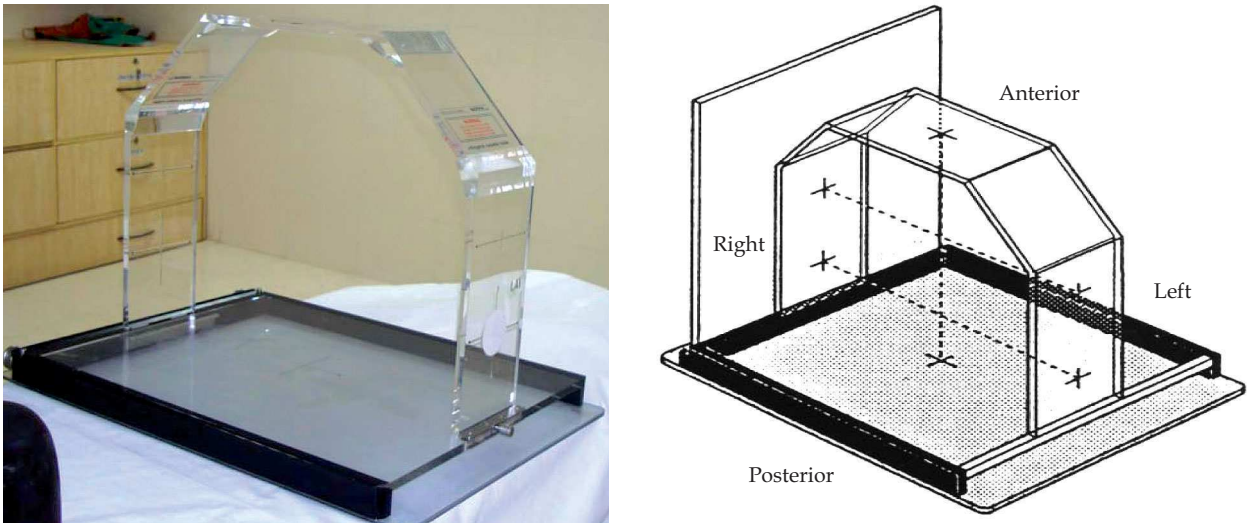

Fig. 1. X-ray images were taken with patient in supine position (AP and lateral views) for conventional planning

doses were planned to keep below 80% of dose to point A for each planned fraction.

3D CT post treatment planning

A CT scan (Somatom Sensation 4, Siemens®) with 3 mm slice thickness through the pelvis was performed for 15 cases out of 30 ICBT insertions. The CT images were transferred to Oncentra Virtual Simulation System (Oncentra MasterPlan version 3.3, Nucletron®) via networking and subsequently to the Plato Treatment Planning System (Nucletron®). The patient was shifted to the treatment chamber and treatment was delivered by MicroSelectron – HDR (Nucletron®) as per the conventional planning. Subsequently the radiation oncologist delineated the bladder and rectum (OARs) in each slice of all the CT images. Although few CT slices contained artefacts, but this was not a serious impediment to contouring bladder and rectum in this study. Rectum was contoured from above the anal sphincter to the level of transition to sigmoid. The entire bladder was contoured. After catheter reconstruction, for each application, the corresponding optimized dwell positions used in conventional 2D planning were duplicated for 3D planning with the contours now drawn. DVH parameters for minimum dose to the most irradiated contiguous volume of 0.1cc, 1cc and 2cc (D0.1cc, D1cc and D2cc, respectively) were produced for each OAR with 100 000 sample points. No contouring was done during actual treatment planning.

Statistical analysis

The paired Student's *t*-test was performed for comparison of ICRU point doses and D2cc volume doses for bladder and rectum. Mean ratio (D2cc/ICRU) was also calculated.

Results

The mean age of the patients was 55 (range 45-60) years. Tumor stage was evaluated according to the International Federation of Gynaecology and Obstetrics (FIGO) classification [7]. The mean contoured volume of bladder and rectum was 104 (± 64) cc and 48 (± 13) cc, respectively. Table 1 shows the mean ICRU point doses and D2cc volume doses for bladder and rectum from this study. The mean D2cc of the bladder obtained from the CT plan was 6.91 Gy (2.9-12.2 Gy). The mean ICRU bladder dose obtained for our patients was 3.08 Gy (1.9-5.9 Gy). Our results reveal that ICRU bladder dose is less than bladder D2cc dose by a ratio of 2.24 (Fig. 3). Mean ICRU and D2cc doses calculated show a statistically significant difference for bladder ($p = 0.000$).

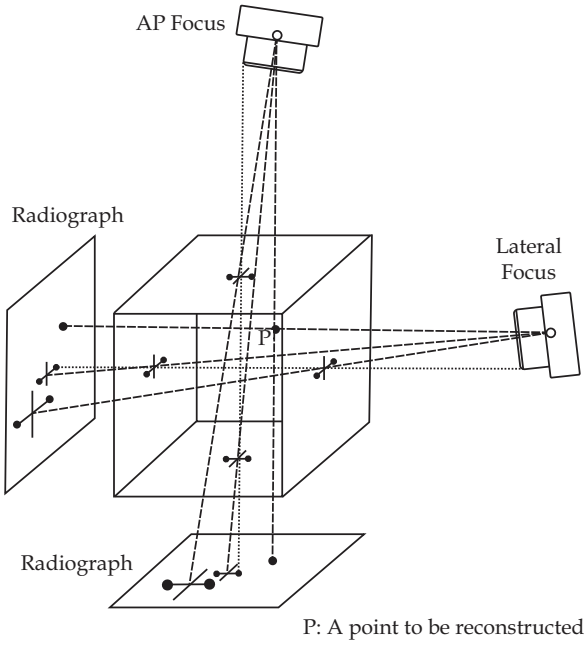

Fig. 2. The semi orthogonal reconstruction method accepts X-rays beams whose central axes do not intersect and are not perpendicular to one another

The mean D2cc of the rectum obtained from the 3D plan was 4.2Gy (2.8-5.9 Gy). The mean ICRU rectal dose obtained from the conventional plan for all patients was 3.8 Gy (2.4-4.45 Gy) (Table 2, Fig. 4). Mean ICRU and D2cc doses calculated did not reveal a statistically significant difference for rectum ($p = 0.08$). The average ratio in this study was 1.10. Physical doses (EBRT+HDR) for OARs at ICRU points as well D2cc were converted to a biologically equivalent dose and normalised to conventional 2Gy ($\alpha/\beta = 3$), EQD2 (Table 3).

Discussion

Intracavitary brachytherapy is an integral part of the treatment of cervical cancer. The treatment planning for the delivery of radiation is dependent on the imaging modality used as well as the method of reconstruction of the applicators and organ at risk. Orthogonal radiographs are traditionally used for treatment planning. However, semi-orthogonal reconstruction especially in the context of C-arm based brachytherapy planning has also been used. There is limited literature available on non-isocentric radiography based intracavitary brachytherapy planning especially

Table 1. Mean ICRU point Doses and D2cc volume doses in bladder and rectum in our study (semi orthogonal method)

	Mean (range) ICRU (Gy)	Mean (range) D2cc (Gy)	Paired *t*-test (range)	Average ratio (D2cc/ICRU)
Bladder	3.08 (1.9-5.9)	6.91 (2.9-12.2)	$p = 0.000$, CI (2.29-5.38)	2.24 ± 1.01
Rectum	3.8 (2.4-4.45)	4.2 (2.8-5.9)	$p = 0.08$, CI (–0.15-0.91)	1.10 ± 0.229

ICRU – International Commission on Radiation Units and Measurements; D2cc – dose received by 2cc of the volume of the bladder calculated from image based CT planning; CI – confidence interval

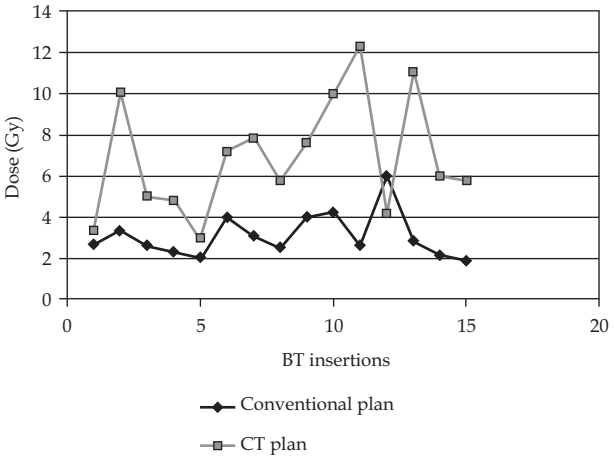

Fig. 3. Comparison of bladder dose by conventional and CT planning

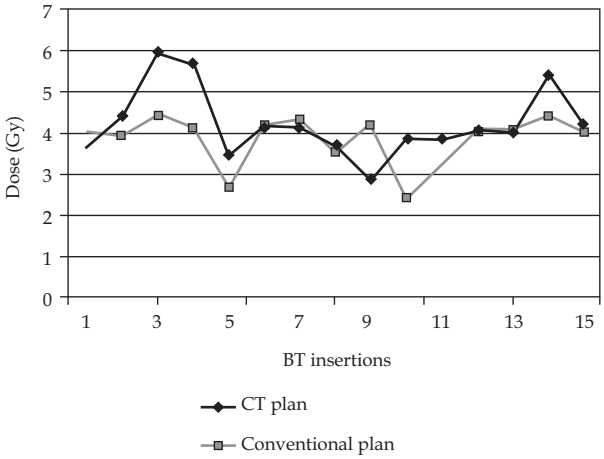

Fig. 4. Comparison of rectal dose by conventional and CT planning

Table 2. Mean ICRU point doses and D2cc volume doses in bladder and rectum (orthogonal method)

	Bladder			Rectum		
	Mean (range) ICRU (Gy)	Mean (range) D2cc (Gy)	Average Ratio (range) (D2cc/ ICRU)	Mean (range) ICRU (Gy)	Mean (range) D2cc (Gy)	Average Ratio (D2cc/ICRU)
Onal *et al.* [12]	6.1 (2.9-8.7)	9.2 (7.6-12.9)	1.51	5 (2.2-10.7)	8.3 (5.1-12.3)	1.66
Jamema *et al.* [13]	4.56	7.12	1.56 ± 0.6	4.63	5.16	1.11 ± 0.2
Tan *et al.* [14]	2.9 (1.2-4.5)	3.9 (1.3-6.3)	1.34 ± 0.34	3.4 (2.4-4.2)	3.6 (1.8-5.9)	1.07 ± 0.25

ICRU – International Commission on Radiation Units and Measurements; D2cc – dose received by 2cc of the volume of the bladder calculated from image based CT planning

Table 3. Biologically normalized total dose EQD2 for bladder and rectum ($\alpha/\beta = 3$) in our study

	OAR'S	
	Bladder Mean (range) (Gy)	Rectum Mean (range) (Gy)
ICRU Point	54 ± 2 (51.8-60.7)	55 ± 1 (52.6-56.6)
D2cc	65 ± 10 (87.5-53.5)	56 ± 2 (53.3-60.6)

Table 4. Comparison of mean ICRU point doses (Gy) for bladder and rectum using semi-orthogonal method and orthogonal method

	Semi-orthogonal method	Orthogonal method	
	Present study (n = 15)	Onal *et al.* [12] (n = 63)	Jamema *et al.* [13] (n = 22)
Point A (Gy)	7	7	7
Bladder Mean (range) (Gy)	3.08 (1.9-5.9)	6.1 (2.9-8.7)	4.56
Rectum Mean (range) (Gy)	4.2 (2.8-5.9)	5 (2.2-10.7)	4.63

n – number of brachytherapy insertions (for a prescription dose of 7 Gy to Point A).

with respect to volumetric dosimetry. Extensive literature is available which clearly suggests that image based brachytherapy is better than point based brachytherapy. The starting point was to retrospectively evaluate our clinical practice by applying 3D assessment of the OARs using CT scans.

Fung [8] has evaluated the reconstruction jig with a C-arm based mobile fluoroscopic unit and found that the jig not only has an excellent accuracy of reconstruction, but it also resolves problems encountered while using C-arm. Both Fung [8] and Cuijpers [9] have suggested that using the jig resolves the problem such as distortion, ill defined planes and sagging, which are issues with image intensifier used in C-arm fluroscopic units. They have reported that the reconstruction jig is narrow and the localization of the marker point becomes difficult for very bulky patients. Nevertheless, in our study our patients did not experience any difficulty in fitting within the jig possibly due to the smaller built of the Indian females as compared to the Western population. In the radiographs taken with the help of reconstruction jig, the bladder and rectal markers were properly visualized in both AP as well as lateral radiographs. However, in some patients the radio opaque markers and contrast in bulb of Foley's catheter were faintly visualized with usual exposure factors and required increasing of the exposure factors (kV, mAs).

For image based dosimetry CT images were used for reconstruction of the applicators. All the patients in this study were treated using standard Fletcher Williamson applicator. The artefacts produced by metal applicators were reduced up to some extent by manipulating the CT window and level setting during CT scan. The accuracy of CT reconstruction was compared with the radiograph based reconstruction of the applicator by overlaying CT reconstruction on radiograph reconstruction. The maximum variation of ± 6 mm was observed between these two with respect to point A. This is attributed to shifting of patient between X-ray room and CT room. It has been shown by Grigsby *et al.* [10] that movement of reference points relative to bony structures during the interval time of two intracavitary implants led to an average shift of 10-15 mm and dose differences of up to 35% were observed due to this high dose gradient. Thomadsen *et al.* [11] have also concluded that any movement of patient should be avoided as this can produce large changes in dose to bladder and rectum.

We compared our results of non isocentric film based ICBT using semiorthogonal reconstruction with the data available in the literature where ICBT was performed with orthogonal reconstruction delivering a dose 7 Gy at similar point A (Table 4). We found that our calculations with semiorthogonal radiographs for bladder and rectal doses were comparable to the doses calculated with orthogonal radiography based studies such as Onal *et al.* [12] (62 HDR applications), Jamema *et al.* [13], (22 HDR applications) (both authors prescribed 7 Gy dose at Point A) as well as with Tan *et al.* [14] (55 applications with 5.3 Gy to Point A). When we compared our results for the mean ICRU point doses obtained using semi orthogonal approach and the D2cc doses for rectum and bladder on CT scans, we found that the average ratio of ICRU rectal dose to D2cc (rectum) by our approach was 1.10 which is similar to the ratios obtained such as 1.66, 1.11 and 1.07 by other authors [12-14] for rectum, respectively. However, the ICRU bladder point underestimated the bladder D2cc dose by a ratio of 2.24 in our study as compared to 1 .51, 1.56 and 1.34 [12-14] (Table 2), but it was comparable with Schoeppel *et al.* [15] and Barillot *et al.* [16]. Other authors such as Hunter *et al.* [17] have also found that the ratio of max bladder dose (from CT images) to ICRU reference dose (calculated from radiographs) varied from 1.01 to 3.59. Schoeppel *et al.* [15] has reported average ratios of 2.3 (range 1.4-2.7) for the bladder and 1.3 (range 0.9-2.1) for the rectum. Barillot *et al.* [16] used ultrasonography for evaluating the bladder doses and found that maximum doses in the bladder were on an average 2.7 times higher than the doses at the ICRU reference points (calculated from radiographs).

Our results are similar with published data for rectal doses, however there is a broad range for bladder doses. Fellner *et al.* [18] has attributed the wide range of ratios for the bladder to different methods used like radiographs, ultrasound, CT to evaluate the doses and the difference in individual patient anatomy.

Conclusions

Treatment planning based on semi-orthogonal films obtained with a non-isocentric X-ray unit with the help of a reconstruction jig is comparable to true orthogonal films on an isocentric X-ray unit. ICRU reference point doses by semiorthogonal reconstruction underestimated the bladder D2cc volume doses, but no significant difference was found for rectum. CT/ MRI based 3D volume based planning should be used wherever feasible as it is better in assessing the doses to OAR volumes than conventional film point based 2D planning and has today become the standard of care in many institutions.

References

1. Atahan I L, Onal C, Ozyar E et al. Long-term outcome and prognostic factors in patients with cervical carcinoma: a retrospective study. *Int J Gynecol Cancer* 2007; 17: 833-842.
2. Nag S. High dose rate brachytherapy: its clinical applications & treatment guidelines. *Technol Cancer Res Treat* 2004; 3: 269-287.
3. Viani GA, Manta GB, Stefano EJ et al. Brachytherapy for cervix cancer: low dose rate or high dose rate Brachytherapy – a meta analysis of clinical trials. *J Exp Clin Cancer Res* 2009; 28: 47.
4. Chassangne D, Duthyerix A, Almond P et al. ICRU Report No.38: Dose & Volume specification for reporting Intracavitary therapy in gynecology. *International Commissioning on Radiation Units & Measurements*, Bethesda 1985.
5. Nag S, Cardenes H, Chang S et al. Proposed guidelines for image-based intracavitary brachytherapy for cervical carcinoma: report from Image-Guided Brachytherapy Working Group. *Int J Radiat Oncol Biol Phys* 2004; 60: 1160-1172.
6. Pötter R, Haie-Meder C, Van Limbergen E et al. Recommendations from gynecological (GYN) GEC ESTRO working group (II); concepts & terms in 3D image based treatment planning in cervix cancer brachytherapy – 3D dose volume parameters and aspects of 3D image based anatomy, radiation physics, radiobiology. *Radiother Oncol* 2006: 78: 67-77.
7. American joint Committee on Cancer, AJCC cancer staging manual. 5th ed. *Lippincott-Raven*, Philadelphia 1997, pp. 259-273.
8. Fung AYC. C-Arm imaging for brachytherapy source reconstruction: Geometrical Accuracy. *Med Phys* 2002; 29: 724-726.
9. Cuijpers JP. Clinical use of a non-isocentric C-arm unit for on line film less reconstruction of brachytherapy applicators. *Radiother Oncol* 2001; 61: 200-209.
10. Grigsby P, Georgiou A, Williamsons J et al. Anatomic variation of gynaecologic brachytherapy prescription points. *Int J Radiat Oncol Biol Phys* 1993; 27: 725-729.
11. Thomadsen B, Shahabi, Stitt J et al. High dose rate intracavitary brachytherapy for carcinoma of the cervix: the Madison System: II, procedural and physical considerations. *Int J Radiat Oncol Biol Phys* 1992; 24: 349-357.
12. Onal C, Arslan G, Topkan E et al. Comparison of conventional and CT based planning for Intracavitary brachytherapy for cervical cancer: target volume coverage and organs at risk doses. *J Exp Clinical Cancer Res* 2009; 28: 95.
13. Jamema SV, Saju S, Mahantshetty U et al. Dosimetric evaluation of rectum and bladder using image based CT planning and orthogonal radiographs with ICRU 38 recommendations in Intracavitary brachytherapy. *J Med Phys* 2008; 33: 3-8.
14. Tan YI, Choo BA, Lee KM. 2D to 3D evaluation of organs at risk doses in intracavitary brachytherapy for Cervical Cancer. *J Contemp Brachyther* 2010; 2: 37-43.
15. Schoeppel S, La Vigne M, Martel M et al. Three dimensional treatment planning of intracavitary gynaecologic implants: analysis of ten cases and implications for dose specification. *Int J Radiat Oncol Biol Phys* 1999; 28: 277-283.
16. Barillot I, Horiot J, Maingon P et al. Maximum and Mean bladder dose defined from ultrasonography: comparison with

the ICRU reference in gynaecological brachytherapy. *Radiother Oncol* 1994; 30: 231-238.
17. Hunter R, Wong F, Moore C et al. Bladder base dosage in patients undergoing intracavitary therapy. *Radiother Oncol* 1986; 7: 189-197.
18. Fellner C, Pötter R, Knocke TH et al. Comparison of radiography and computed tomography based treatment planning in cervix cancer in brachytherapy with specific attention to some quality assurance aspect. *Radiother Oncol* 2001; 58: 53-62.

ELSEVIER

CrossMark

BRACHYTHERAPY

Brachytherapy 14 (2015) 578–585

Radiochromic film–based quality assurance for CT-based high-dose-rate brachytherapy

Saeid Asgharizadeh[1,2], Hamed Bekerat[1,2], Alasdair Syme[1,2], Saad Aldelaijan[1,2], François DeBlois[1,2], Té Vuong[2], Michael Evans[1,3], Jan Seuntjens[1], Slobodan Devic[1,2,*]

[1]*Medical Physics Unit, McGill University, Montréal, Québec, Canada*
[2]*Department of Radiation Oncology, Jewish General Hospital, McGill University, Montréal, Québec, Canada*
[3]*Department of Medical Physics, McGill University Health Centre, Montréal, Québec, Canada*

ABSTRACT

PURPOSE: In the past, film dosimetry was developed into a powerful tool for external beam radiotherapy treatment verification and quality assurance. The objective of this work was the development and clinical testing of the EBT3 model GafChromic film based brachytherapy quality assurance (QA) system.

METHODS AND MATERIALS: Retrospective dosimetry study was performed to test a patient-specific QA system for preoperative endorectal brachytherapy that uses a radiochromic film dosimetry system. A dedicated phantom for brachytherapy applicator used for rectal cancer treatment was fabricated enabling us to compare calculated-to-measured dose distributions. Starting from the same criteria used for external beam intensity-modulated radiation therapy QA (3%, 3 mm), passing criteria for high- and low-dose gradient regions were subsequently determined. Finally, we investigated the QA system's sensitivity to controlled source positional errors on selected patient plans.

RESULTS: In low-dose gradient regions, measured dose distributions with criteria of 3%, 3 mm barely passed the test, as they showed 95% passing pixels. However, in the high-dose gradient region, a more stringent condition could be established. Both criteria of 2%, 3 mm and 3%, 2 mm with gamma function calculated using normalization to the same absolute dose value in both measured and calculated dose distributions, and matrix sizes rescaled to match each other showed more than 95% of pixels passing, on average, for 15 patient plans analyzed.

CONCLUSIONS: Although the necessity of the patient-specific brachytherapy QA needs yet to be justified, we described a radiochromic film dosimetry–based QA system that can be a part of the brachytherapy commissioning process, as well as yearly QA program.

Keywords: Radiochromic film dosimetry; Quality assurance; Brachytherapy

Introduction

Brachytherapy represents clinical use of small encapsulated radioactive sources at short distances from target volumes for irradiation of both malignant tumors and benign lesions. Brachytherapy methods vary considerably depending on their complexity and the scope to which they are individualized to particular patients. The aim of a brachytherapy quality assurance (QA) program should be to maximize the likelihood that each treatment is administered accurately, recognizing the clinical intent and that it is performed safely for both the patient and others who might be exposed to radiation during the treatment. With the advancements in brachytherapy treatment techniques, the need for comprehensive QA programs has been recognized (1), and the number of QA tools and procedures has been summarized in numerous recommendation documents (2–4). In addition, within the last decade, the brachytherapy community witnessed a widespread use of various image guidance techniques and with it new challenges for brachytherapy QA programs (5, 6).

The absence of patient-specific QA process in brachytherapy is in contrast with the situation for intensity-modulated radiation therapy (IMRT) where this is a standard practice. External beam–based IMRT uses specialized computer-driven technology to create dose distributions that

Received 25 November 2014; received in revised form 9 January 2015; accepted 8 February 2015.

* Corresponding author. Medical Physics Unit, McGill University, Jewish General Hospital, 3755 Cote St-Catherine, Montreal, Québec, Canada H3T 1E2. Tel.: +1-514-340-8222/2595; fax: +1-514-340-8642.

E-mail address: slobodan.devic@mcgill.ca (S. Devic).

1538-4721/$ - see front matter
http://dx.doi.org/10.1016/j.brachy.2015.02.192

conform to tumor targets with extremely high precision (7). The generated conformal dose distributions around the tumor can have steep dose gradients at the transition to adjacent healthy tissues, similar to those commonly encountered in brachytherapy treatments. IMRT technique has been discussed in detail in the literature covering technical, physical, and clinical aspects (8, 9). Numerous publications (10–12) outlined the importance of performing comprehensive acceptance testing, commissioning, and QA programs for IMRT. A number of methods, techniques, and detector systems have been designed for patient-specific IMRT verification purposes, where both dosimetric and spatial uncertainties are determined (13–15).

From the point of view of the equipment used, brachytherapy uses a rather simple technology, in the form of driving an encapsulated radioactive source to preplanned dwell positions to spend preplanned dwell times. On the other hand, brachytherapy procedures involve procedures performed by different professionals (radiation oncologists, physicists, therapists, and others), each of which can represent a potential source of treatment error. Possible mistakes during the process of CT-based planned brachytherapy procedures could occasionally lead to serious faults, thus undermining the treatment goals. Possible adverse effects may be further amplified as brachytherapy is given over one or only few fractions (16).

The use of radiochromic films for dose measurements in brachytherapy dates back to the work by Sayeg and Gregory (17) who measured surface dose rates with high-dose-rate (HDR) beta particle ophthalmic applicators. Sharma *et al.* (18) used radiochromic films to measure the anisotropy function of iridium-192 (^{192}Ir) brachytherapy sources. Poon *et al.* (19) modeled the intracavitary mold applicator used for endorectal cancer brachytherapy treatments for Monte Carlo–simulated dose calculations subsequently verified using the external beam therapy (EBT) film model. Evans *et al.* (20) introduced a QA check for source positioning using radiochromic instead of traditional radiographic film.

In the case of IMRT-based dose evaluation, the gamma index is often used to quantify differences between two dose distributions (21): one calculated by the treatment planning system (TPS) and another one measured by the appropriate QA tool. The gamma function quantifies a quadratic combination of the distance-to-agreement (DTA) metric between two dose distributions with a point dose–difference metric. A passing criterion can be established that determines that a particular number of evaluation points (usually 95%) satisfy a combined dose difference (DD) and DTA threshold (e.g., 5%, 2 mm). Following the same approach as in the case of IMRT QA, Devic *et al.* (22) reported on the possible use of radiochromic film–based dosimetry system for HDR quality control and commissioning.

In this work, we describe a potential patient-specific QA system for fractionated preoperative HDR ^{192}Ir brachytherapy treatments for rectal cancer patients. The patient-specific QA tool developed here relies on the radiochromic film dosimetry system and the gamma evaluation method for quantitative evaluation of dose distributions. To investigate the eventual need for patient-specific QA in brachytherapy practice, we performed a retrospective dosimetry study on 15 CT-based rectal treatment plans. The QA system described was used to compare dose distributions calculated using Task Group No. 43 formalism (23) with those measured by the EBT3 model GafChromic film–based reference dosimetry system using a specially designed brachytherapy QA phantom. We also investigated the QA system's sensitivity to source positional errors by introducing intentional and controlled offsets on selected patient plans.

Methods and materials

Radiochromic film dosimetry protocol

In this study, we used the latest EBT3 GafChromic film model (Ashland Inc., Wayne, NJ) that provides two significant performance improvements over the EBT2 film model. Although the active layer in the two film models remains the same, the EBT3 film model has a unique polyester substrate that prevents the formation of Newton's rings interference patterns in images acquired using flatbed document scanners (24). Furthermore, as opposed to the EBT2 film model that has an asymmetric structure of layers, the EBT3 film model has a 30-μm thick active layer sandwiched between two mated 125-μm thick polyester sheets.

All films used in this work were from the same batch number (A05151202). The reading device used was a flatbed Epson Expression 10000XL document scanner (Epson, Nagano, Japan) that provides 48-bit red, green, and blue images scanned in transmission mode. In this work, we used reference radiochromic film dosimetry protocol described by Aldelaijan *et al.* (25) with the calibration irradiation setup using parallel-opposed beam geometry. As shown, the main advantage of this irradiation setup was to achieve a greater degree of dose homogeneity in the region of interest (ROI) within the phantom where the calibration film pieces are positioned. Fifteen calibration film pieces ($2'' \times 2.5''$) were exposed to various doses in a range between 25 and 3000 cGy. All films were scanned with a 127 dpi resolution, which corresponds to 0.2 mm/pixel. Discontinued FilmQA software (3cognition LLC, version 2.0.1215) was used to analyze irradiated and 24 h postexposure scanned film pieces, and based on the anticipated dose range used in this study (0–30 Gy), we decided to use the green color channel (25). We also tested the latest triple-channel film analysis approach (26) using the FilmQAPro (Ashland, Inc., Wayne, NJ) software.

Figure 1 shows the calibration curve (a), as well as the uncertainty vs. error analysis (b) for the reference radiochromic film dosimetry system used in this work. As expected, dose errors (calculated as the difference between known and calculated dose) and dose uncertainties (sum

of experimental and fitting uncertainties (25)) are higher at lower dose values. The larger dose errors at lower dose values will eventually result in more significant discrepancies between calculated and measured doses within low-dose regions when gamma function is calculated. The uncertainty vs. error analysis (Fig. 1, b) suggests that the radiochromic film dosimetry system used in this work is consistent with its one sigma uncertainty estimate because the error points are larger than the uncertainty values in less than 33% of cases and provides a one sigma uncertainty better than 3% in a dose range of up to 30 Gy.

HDR brachytherapy QA phantom

Design of a solid water phantom with an intracavitary mold applicator (Nucletron, Veenendaal, The Netherlands) positioned at its center is shown in Fig. 2. The applicator is made of silicon rubber and has a length of 28 cm, a 24 mm diameter, and a flexible cylindrical shape. Eight catheters are placed within its circumference around a central cavity designed to accommodate a tandem catheter for gynecological brachytherapy applications. The brachytherapy QA phantom consists of four solid water slabs (Fig. 2). One slab has dimensions of 30 × 30 × 2 cm^3, and the second one has dimensions of 30 × 30 × 5 cm^3, and the two slabs are milled to accommodate the applicator in the center. Two additional

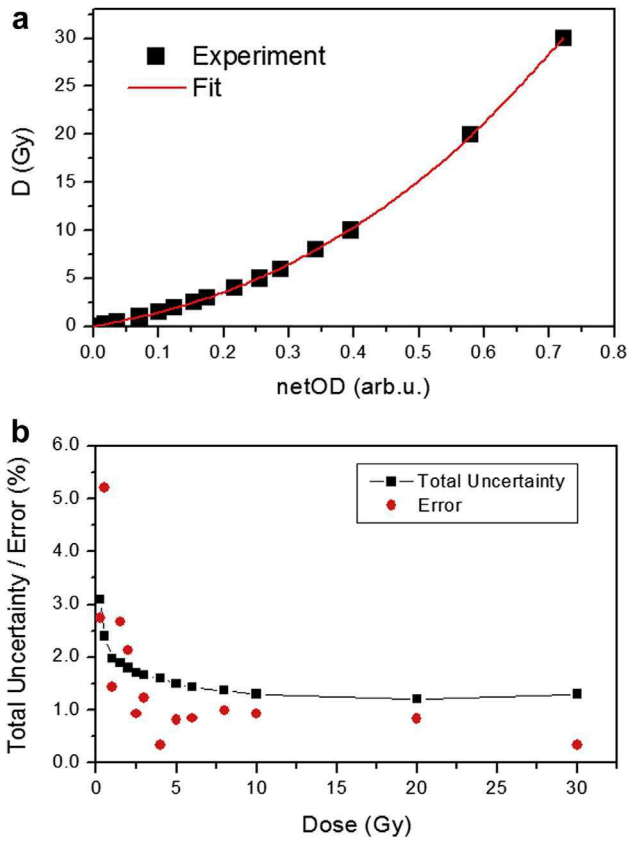

Fig. 1. (a) Calibration curve and (b) dose error vs. total uncertainty for the reference radiochromic film dosimetry system used in this work.

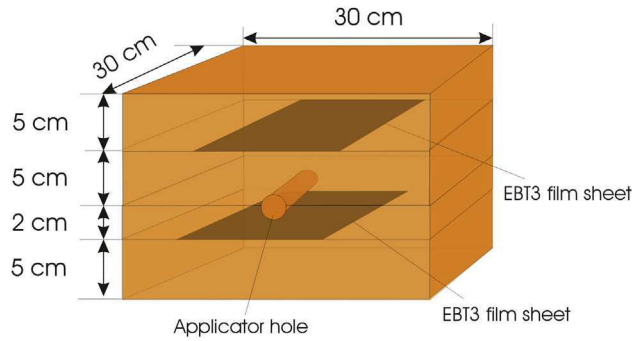

Fig. 2. High-dose-rate brachytherapy phantom for rectal cancer patients. Applicator is centered in the phantom. Two GafChromic films are positioned 2 cm below and 5 cm above the center of the applicator. Film dimensions not to scale.

slabs of solid water with dimensions 30 × 30 × 5 cm^3 are added above and below to provide full scattering conditions. According to the latest American Association of Physicists in Medicine Task Group No. 43 update (23), every point of calculation and/or measurement must be surrounded by at least 5 cm of water-equivalent material. In designing the phantom depicted in Fig. 2, we made sure that every film measurement point within the ROI, defined in the next section, was surrounded by at least 5 cm of solid water material. Finally, the two central slabs of solid water are attached together with plastic screws to assure that the applicator would not move during dose delivery.

During QA measurements, two sheets of EBT3 model GafChromic film were placed 2 cm above and 5 cm below the center of the applicator to measure dose distributions within high- and low-dose gradient regions, respectively. To ensure films were positioned inside the phantom in a reproducible manner, we used a permanent marker to draw an area that defines the film size on two slabs of solid water.

Radiochromic film–based brachytherapy QA analysis

Figure 3 outlines basic steps in the proposed radiochromic film–based brachytherapy QA system that mimics the well-established IMRT QA procedure using the same dosimetry system. The three-dimensional dose distribution of each treatment plan was recalculated with brachytherapy treatment planning software using a CT image data set of the QA phantom. Dwell times and dwell positions for each plan were re-entered manually to the QA (mock) plan created within Masterplan (version 4.1; Nucletron, Veenendaal, The Netherlands). Two planar dose distributions positioned at 2 cm below and 5 cm above the center of the applicator were exported as a Digital Imaging and Communications in Medicine dose file and subsequently imported into FilmQA software (Fig. 3a).

Next, the scanned (digitized) film images created using the mock plan was imported as Tiff files into the FilmQA software (Fig. 3b) and coregistered to the calculated dose distribution. Alignment is achieved by lining up permanent

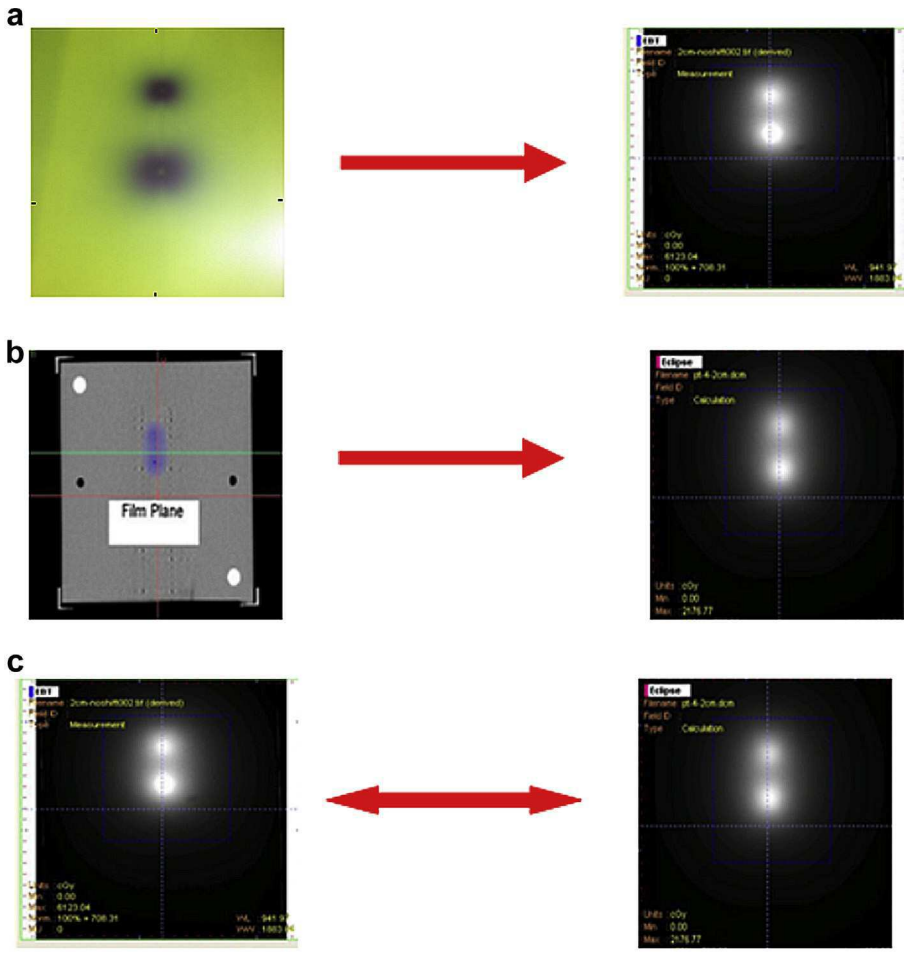

Fig. 3. The procedure for the comparison of the measured dose distribution with the calculated one. (a) Measured netOD distribution converted to dose image. (b) Calculated dose distribution converted to dose image. (c) Two dose images are coregistered and compared.

fiducial marks on the phantom (drawn by permanent marker and aligned to the first dwell position of the applicator) to fiducial marks (created using a permanent marker) on the film sheet. However, because of several sources of uncertainties in this method (estimated to be within 1 mm) during gamma function analysis, we used manual dose adjustment option (with a step size of 0.1 mm) to maximize passing rate of the function by moving film dose distribution with respect to calculated one, assuming that the shifts are not larger than 1 mm.

Before comparing the two dose distributions using the gamma function (Fig. 3c), the scanned film image is converted into an absolute dose image using previously established calibration curve. To reduce the level of noise in film measurements because of low-dose values measured (usually away from the center of the dose distribution), gamma function calculations were confined to an ROI, defined as an area with doses in excess of 30% of the maximum dose calculated by the TPS.

For this study, we selected treatment plans for 15 rectal cancer patients treated preoperatively with HDR brachytherapy. The treatment is delivered in four daily fractions (with a prescription dose of 6.5 Gy to the target volume per fraction) within the four consecutive days after the CT simulation and treatment planning. Before each treatment fraction, the applicator is inserted into the rectal lumen, and a radiograph is taken for comparison with the reference digitally reconstructed radiograph, created based on planning CT. Comparison of the two radiographs is carried out to determine corrections (if any) needed to assure that the treatment plan, created using planning CT, is delivered to the target in a reproducible manner during all treatment fractions. Details of this image-guided brachytherapy (IGBT) technique have been described in details previously (26). For most of the IGBT techniques (rectum, head and neck, breast, surface), fractionation allows for eventual implementation of patient-specific QA because the time between CT simulation and first treatment fraction is usually 1 day, as it is the case for IMRT. However, a large number of brachytherapy procedures (gynecology, prostate, and esophagus) are adaptive (daily imaging and planning before treatment delivery) and do not provide enough time for such QA programs. Instead, the adaptive brachytherapy techniques may benefit from the implementation of *in vivo* patient-specific QA (27). On the other hand, taking into

account the relative technical simplicity of brachytherapy dose delivery and recent reporting on the usefulness of patient-specific QA for IMRT (28), additional retrospective dosimetry studies (similar to ours) may prove that *in vivo* patient-specific QA could be the only meaningful path toward brachytherapy quality care improvement for fractionated IGBT as well.

When choosing treatment plans for this study, we tried to avoid repetitive combinations of channels in the applicator to collect plans covering different dose distributions. Although most treatment plans created and delivered use only three channels, we have made sure these are distributed in our sample group around all aspects around the applicator (ANT, POST, LT, and RT). In addition, we also included three plans (ANT, POST, and LT) with four catheters. For each treatment plan, we compared the calculated planar dose distributions with measured ones using the gamma function method, which combines two mapping criteria of DDs and DTAs. In this work, we altered the criterion for DD to be 1%, 2%, and 3%, whereas the criterion for DTA was changed to be 1, 2, and 3 mm.

Commonly in IMRT QA practice, both measured and calculated dose distributions are converted to relative dose images being normalized to the origin point set at the center of the calculated dose distribution matrix. However, such method provides comparison (in terms of the gamma function passing criteria) of relative dose distributions only. In the case of an incorrectly used activity, for dose calculation such a comparison would not be detected by such a system. In the case of IMRT QA, this problem was alleviated by the use of ionization chamber measurements in parallel to the film measurement within the same phantom. To test the ability of the radiochromic film system in providing comparison between absolute dose distributions, we calculated gamma function by normalizing both calculated and measured dose distributions to the very same absolute dose value equal to the maximum dose taken from the calculated dose distribution, the later one assumed to be a reference. Only in such a way, can the two dose distributions be compared in terms of absolute dose if the gamma function is used for comparison.

Another technical detail frequently overlooked in the process of IMRT QA is the difference in pixel resolutions between measured (with film) and calculated (with TPS) dose distributions. In our case, we have used the scanning pixel size of 0.2 mm/pix (commonly used during our IMRT QA), whereas the pixel size in the calculated dose distribution was 2 mm/pix. To assess the impact of different pixel sizes of dose distributions used for gamma function calculation, we had also resampled the film-measured dose distribution of 0.2 to 2 mm/pix.

Finally, to investigate the sensitivity of our film–based brachytherapy QA system to positional errors of the ^{192}Ir source, we selected three patient plans and introduced deliberate errors of 1, 2, 3, and 5 mm, for one dwell position, in one channel at the treatment console and delivered the erred plan to the QA phantom containing radiochromic films. Measured dose distributions were then compared with the calculated one for a given treatment plan. The resulting change in average passing pixels (APPs) of the gamma maps will be used to describe the sensitivity of our QA system to this intentional positional error.

Results and discussion

Gamma evaluation for high- and low-dose regions

Table 1 summarizes the average values of passing pixels (APP) for high- and low-dose gradient areas, respectively. The first column within a given dose gradient area corresponds to APP when dose distributions were normalized to the center values separately (corresponding to relative dose distribution comparison via gamma map), and measured and calculated dose matrices had different pixel sizes. The second column (labeled renormalized) corresponds to APP of gamma functions calculated using relative dose distributions in two dose images (calculated and measured) normalized to the very same dose value (absolute dose comparison) corresponding to the maximum absolute dose value of dose distribution calculated within the plane containing the film. The third column for both dose gradient regions corresponds to the gamma function calculated based on absolute dose comparison and the measurement dose image rescaled to match the pixel size of the calculated dose image. Finally, the last column for both dose gradient regions incorporates the triple-channel radiochromic film dosimetry method (29).

Results presented in Table 1 suggest that the variation of the DTA parameter has more influence on gamma map passing pixels in the high-dose gradient area (film at plane 2 cm from the center of the applicator). In contrast, it can be seen that the DD parameter will have more influence on the percentage of the passing pixels in a low-dose gradient region (film at plane 5 cm from the center of the applicator). On the other hand, introduction of dose distribution normalization to the same dose value (absolute dose comparison) slightly improves the APP in the high-dose gradient region, contrary to the trend in the low-dose gradient region. This might be caused by the fact that the uncertainty in absolute dose measured with the film decreases as the dose is increased (25). Rescaling of the high-resolution dose measurements image to calculated low-resolution dose image resulted in an overall reduction in APP for all cases. In the case of the FilmQA software, and in other commercially available software packages, the calculated low-resolution dose distribution image is oversampled to match the high resolution of the film measurement. Our results confirm previously published data (30, 31) that such an approach may lead to an unjustified overconfidence in the calculated gamma function. Although the scanning resolution of the film image should be as close as possible to the dose calculation grid size, one should at least match the high-resolution image to the low-resolution

Table 1
APPs for a different combination of DTA and DD criteria in high (film at 2 cm) and low-dose gradient region (film at 5 cm)

Criteria	High-dose gradient region (film at 2 cm)				Low-dose gradient region (film at 5 cm)			
DD, DTA	Original	Renormalized	Renormalized & rescaled	Renormalized & rescaled & triple channel	Original	Renormalized	Renormalized & rescaled	Renormalized & rescaled & triple channel
1%, 1 mm	65.3	76.5	51.7	32.3	65.1	52.1	24.6	22.2
1%, 2 mm	85.3	91.9	81.9	81.5	79.4	63.3	38.9	46.2
1%, 3 mm	92.2	96.8	94.3	95.3	86.9	70.5	54.1	71.4
2%, 1 mm	73.1	85.5	70.2	62.3	76.2	62.9	39.3	43.0
2%, 2 mm	89.5	94.9	88.5	92.9	85.7	70.9	50.1	62.9
2%, 3 mm	95.1	97.8	97.2	97.2	90.9	75.8	62.1	83.2
3%, 1 mm	79.9	92.4	83.6	79.8	83.9	70.8	54.8	68.1
3%, 2 mm	92.4	96.9	94.4	96.0	89.6	77.1	62.4	83.6
3%, 3 mm	95.9	98.6	98.4	98.2	95.3	81.1	70.1	92.0

APPs = average passing pixels; DTA = distance to agreement; DD = dose difference.

one, and not vice versa. Introduction of the triple-channel method leads to a significant increase in the pixel passing rate within low-dose gradient region when compared with the rescaled images approach, albeit still below 95%, showing that the method improves dose measurements analysis in dose regions with higher noise levels. In the high-dose gradient region, the impact of triple channel appears to be less significant, yet achieving the 95% passing rate for 1%, 3 mm criterion.

Positional source errors measurements

Figure 4 shows the percentage of APPs for the gamma function calculated using different DTA parameters affected by introducing positional errors for one dwell position of 1, 2, 3, and 5 mm in 3 selected patients. On average, plans had 56 dwell positions over three channels, with 2.5-mm step size. This figure further suggests that in the high-dose region, the introduction of positional errors greater than 1 mm leads to a significant reduction of the passing pixel rate. Although the introduction of a 1-mm source shift had no significant impact on the percentage of passing pixels for 3%, 3 mm criteria, even this smallest error was already registered by more stringent 3%, 2 mm criteria resulting in a significant drop in passing pixels from 100% to 85%. Figure 4 also reveals that a source positional error of 2 mm decreased the percentage of passing pixels significantly well below 60% for all the DD/DTA combinations tested, indicating that the system described in this work can detect positional errors larger than 1 mm.

Summary of radiochromic film–based QA system for brachytherapy

Figure 5 represents the summary of the proposed radiochromic film dosimetry QA system. The system relies on an initial scanning of the QA phantom and established calibration curve for a given radiochromic film dosimetry system. For every new radiochromic film batch, a new calibration curve has to be created. The end-to-end test starts with the transfer of the treatment plan onto a CT data set of

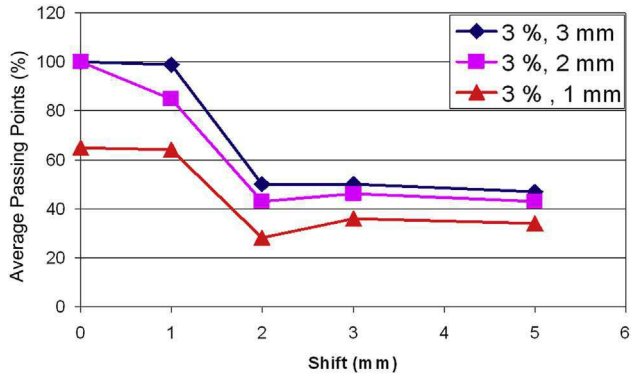

Fig. 4. Effect of positional errors in average passing pixels in high-dose region.

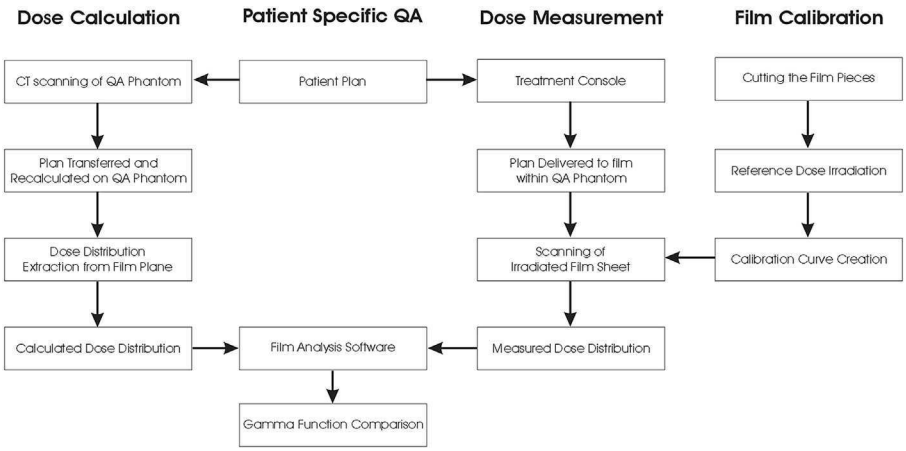

Fig. 5. Summary of the proposed radiochromic film–based brachytherapy quality assurance (QA) system.

the QA phantom and recalculation of the dose distribution that is intended to be delivered to the patient.

The very same plan is also sent to the treatment console and delivered to radiochromic film sheets placed within the QA phantom at predefined positions. Dose distribution corresponding to the film position is exported from a recalculated plan and imported into film analysis software together with the measured dose distribution. Two dose distributions are subsequently compared using the gamma function.

Conclusions

In this work, we tested a radiochromic film–based QA procedure for patient-specific QA of HDR brachytherapy. Two films were positioned at 2 cm below and 5 cm above the center of an endorectal brachytherapy applicator within a QA phantom. These two films were used to study the behavior of the QA system in low- and high-dose gradient regions.

The gamma evaluation method was used to evaluate dose distributions for the case of preoperative endorectal brachytherapy treatments based on radiochromic film dosimetry. In low-dose gradient regions, measured dose distributions with criteria of 3%, 3 mm barely passed the test as they showed 95% passing pixels for the oversampled and relative dose distribution comparison. However, in the high-dose gradient region, a more stringent condition could be established. Both criteria of 2%, 3 mm and 3%, 2 mm with gamma function calculated using normalization to the same absolute dose value in both measured (using triple-channel method) and calculated dose distributions and matrix sizes rescaled to match lower resolution (calculated dose image) showed more than 95% pixels passing on average for 15 patient plans used.

We also demonstrated that the QA system described when used in conjunction with preoperative endorectal HDR brachytherapy is sensitive to source positional errors. We investigated the effect of the positional errors on the percentage of passing pixels and concluded that introducing a positional error for one dwell position within one channel larger than 1 mm will decrease the average percentage of the passing pixels at a level that is significant and detectable.

In this work, we described a radiochromic film–based brachytherapy QA system, which could be used as a patient-specific QA tool if the treatment protocol allows for a sufficient time and resources to undertake all the steps similar to well-established IMRT QA. However, the necessity of patient-specific QA program in brachytherapy should be assessed with regard to the ongoing discussion whether the very same patient-specific QA programs should be continued and/or changes for IMRT toward process-specific QA program. Additional retrospective dosimetry studies (similar to this one) may prove that *in vivo* patient-specific QA could be the only meaningful path toward brachytherapy quality care improvement for both IGBT and adaptive CT-based fractionated brachytherapy techniques. On the other hand, the system described in this work could be readily used for regular QA tests (e.g., after a source change) and/or during the process of commissioning of the new brachytherapy program in the clinic.

Acknowledgments

This work was supported by the Natural Sciences and Engineering Research Council of Canada Contract No. 386009. SD is a Senior Research Scientist supported by the Fonds de Recherche en Santé du Québec 26856.

References

[1] Slessinger E, Grigsby PW, Williams J. Improvements in brachytherapy quality assurance. *Int J Radiat Oncol Biol Phys* 1989;16:497–500.
[2] Nath R, Anderson LL, Meli JA, *et al*. Code of practice for brachytherapy physics: Report of the AAPM Radiation Therapy Committee Task Group No. 56. *Med Phys* 1997;24:1557–1598.
[3] Valentin J. Prevention of high-dose-rate brachytherapy accidents. ICRP Publication 97. *Ann ICRP* 2005;35:1–51.

[4] Butler WM, Merrick GS. Clinical practice and quality assurance challenges in modern brachytherapy sources and dosimetry. *Int J Radiat Oncol Biol Phys* 2008;71:S142–S146.
[5] Williamson JF. Current brachytherapy quality assurance guidance: Does it meet the challenges of emerging image-guided technologies? *Int J Radiat Oncol Biol Phys* 2008;71:S18–S22.
[6] Cormack RA. Quality assurance issues for computed tomography-, ultrasound-, and magnetic resonance imaging-guided brachytherapy. *Int J Radiat Oncol Biol Phys Phys* 2008;71:S136–S141.
[7] Bortfeld T, Schmidt-Ullrich R, De Neve W, *et al*. *Image-guided IMRT*. Berlin, Germany: Springer; 2006. p. 1041.
[8] Webb S. The physical basis of IMRT and inverse planning. *Br J Radiol* 2003;76:678–689.
[9] Staffurth JA. Review of the clinical evidence for intensity-modulated radiotherapy. *Clin Oncol* 2010;22:643–657.
[10] Van Esch A, Bohsung J, Sorvari P, *et al*. Acceptance tests and quality control (QC) procedures for the clinical implementation of intensity modulated radiotherapy (IMRT) using inverse planning and the sliding window technique: Experience from five radiotherapy departments. *Radiother Oncol* 2002;65:53–70.
[11] Van Zijtveld M, Dirkx MLP, de Boer HCJ, *et al*. Dosimetric pretreatment verification of IMRT using an EPID; clinical experience. *Radiother Oncol* 2006;81:168–175.
[12] Warkentin B, Steciw S, Rathee S, *et al*. Dosimetric IMRT verification with a flat-panel EPID. *Med Phys* 2003;30:3143–3155.
[13] Low DA, Harms WB, Mutic S, *et al*. A technique for the quantitative evaluation of dose distributions. *Med Phys* 1998;25:656–661.
[14] De Wagter C. *QA-QC of IMRT—European perspective. Image-guided IMRT*. Berlin, Heidelberg, Germany: Springer; 2006. p. 117–128.
[15] Molineu A, Followill DS, Balter PA, *et al*. Design and implementation of an anthropomorphic quality assurance phantom, for intensity-modulated radiation therapy for the Radiation Therapy Oncology Group. *Int J Radiat Oncol Biol Phys* 2005;63:577–583.
[16] Thomadsen B, Lin SW, Laemmrich P, *et al*. Analysis of treatment delivery errors in brachytherapy using formal risk analysis techniques. *Int J Radiat Oncol Biol Phys* 2003;57:1492–1508.
[17] Sayeg JA, Gregory RC. A new method for characterizing beta-ray ophthalmic applicator sources. *Med Phys* 1991;18:453–461.
[18] Sharma SD, Bianchi C, Conte L, *et al*. Radiochromic film measurement of anisotropy function for high-dose-rate Ir-192 brachytherapy source. *Phys Med Biol* 2004;49:4065–4072.
[19] Poon E, Reniers B, Devic S, *et al*. Dosimetric characterization of a novel intracavitary mold applicator for Ir-192 high dose rate endorectal brachytherapy treatment. *Med Phys* 2006;33:4515–4526.
[20] Evans M, Devic S, Podgorsak EB. High dose-rate brachytherapy source position quality assurance using radiochromic film. *Med Dosim* 2007;32:13–15.
[21] Low DA, Dempsey JF. Evaluation of the gamma dose distribution comparison method. *Med Phys* 2003;30:2455–2464.
[22] Devic S, Tomic N, DeBlois F. Brachytherapy TPS QA using EBT model GafChromic film. *Med Phys* 2009;36:2528.
[23] Rivard MJ, Coursey BM, DeWerd LA, *et al*. Update of AAPM Task Group No. 43 Report: A revised AAPM protocol for brachytherapy dose calculations. *Med Phys* 2004;31:633–674.
[24] Reinhardt S, Hillbrand M, Wilkens JJ, *et al*. Comparison of Gafchromic EBT2 and EBT3 films for clinical photon and proton beams. *Med Phys* 2012;39:5257–5262.
[25] Aldelaijan S, Mohammed H, Tomic N, *et al*. Radiochromic film dosimetry of HDR 192Ir source radiation fields. *Med Phys* 2011;38:6074–6083.
[26] Devic S, Vuong T, Moftah B, *et al*. Image guided high dose rate endorectal brachytherapy. *Med Phys* 2007;34:4451–4458.
[27] Tanderup K, Beddar S, Andersen CE, *et al*. In vivo dosimetry in brachytherapy. *Med Phys* 2013;40:070902.
[28] Kry SF, Molineu A, Kerns JR, *et al*. Institutional patient-specific IMRT QA does not predict unacceptable plan delivery. *Int J Radiat Oncol Biol Phys* 2014;90:1195–1201.
[29] Lewis D, Micke A, Yu X, *et al*. An efficient protocol for radiochromic film dosimetry combining calibration and measurement in a single scan. *Med Phys* 2012;39:6339–6350.
[30] Nelms BE, Simon JA. A survey on planar IMRT QA analysis. *J Appl Clin Med Phys* 2007;8:76–90.
[31] Baileya DW, Nelms EB, Attwood K, *et al*. Statistical variability and confidence intervals for planar dose QA pass rates. *Med Phys* 2011;38:6053–6064.